AFRL-VS-HA-TR-98-0121

Parallel Developments in Theoretical Modeling, Empirical Modeling, and Ionospheric Data Analyses

Matthew W. Fox

Boston University
Center for Space Physics
725 Commonwealth Avenue
Boston, MA 02215

December 1998

AIR FORCE RESEARCH LABORATORY
Space Vehicles Directorate
29 Randolph Rd
AIR FORCE MATERIEL COMMAND
Hanscom AFB, MA 01731-3010

" This technical report has been reviewed and is approved for publication."

KEVIN P. RAY
Contract Monitor

GREGORY P. GINET, Chief
Space Weather Center of Excellence

This report has been reviewed by the ESC Public Affairs Office (PA) and is releasable to the National Technical Information Service (NTIS).

Qualified requestors may obtain additional copies from the Defense Technical Information Center (DTIC). All others should apply to the National Technical Information Service (NTIS).

If your address has changed, if you wish to be removed from the mailing list, of if the addressee is no longer employed by your organization, please notify PL/IM, 29 Randolph Road, Hanscom AFB, MA. 01731-3010. This will assist us in maintaining a current mailing list.

Do not return copies of this report unless contractual obligations or notices on a specific document require that it be returned.

REPORT DOCUMENTATION PAGE

Form Approved
OMB No. 0704-0188

1. REPORT DATE *(DD-MM-YYYY)*	2. REPORT TYPE	3. DATES COVERED *(From - To)*
December 1998	Scientific, Interim	Apr 97-Oct 98

4. TITLE AND SUBTITLE
Parallel Developments in Theoretical Modeling, Empirical Modeling and Ionospheric Data Analyses

5a. CONTRACT NUMBER
F19628-97-C-0034

5b. GRANT NUMBER

5c. PROGRAM ELEMENT NUMBER
35160F

6. AUTHOR(S)
Matthew W. Fox

5d. PROJECT NUMBER
SMPS

5e. TASK NUMBER
GL

5f. WORK UNIT NUMBER
88

7. PERFORMING ORGANIZATION NAME(S) AND ADDRESS(ES)
Boston University
Center for Space Physics
725 Commonwealth Avenue
Boston, MA 02215

8. PERFORMING ORGANIZATION REPORT NUMBER

9. SPONSORING/MONITORING AGENCY NAME(S) AND ADDRESS(ES)
Air Force Research Laboratory
29 Randolph Rd
Hanscom AFB, MA 01731-3010

10. SPONSOR/MONITOR'S ACRONYM(S)

11. SPONSOR/MONITOR'S REPORT NUMBER(S)
AFRL-VS-HA-TR-98-0121

12. DISTRIBUTION/AVAILABILITY STATEMENT
Approved for Public Release; distribution unlimited

13. SUPPLEMENTARY NOTES

14. ABSTRACT
In this report, we describe a number of ionospheric studies, involving variously theoretical models, empirical models, and data analyses. All are ultimately geared towards Air Force objectives of monitoring and specification of the ionospheric environment. A new multiple-ion theoretical model has been examined with a view to both describing the morphology of light ionos, and validating the model by comparisons with observational data. Further, a version of the code has been developed to model geomagnetic disturbances at low latitudes utilizing a new empirical dynamo disturbance drift model. Applications of an empirical profile shape model are being developed including: its ability to summarize profiles generated by the spedcification model, PIM; its potential in guiding thedevelopment of a new slant to vertical TEC conversion; and its potential use in adapting profile specifications with real-time data adjustments. Finally, data analyses have been undertaken to investigate the nature of quiet-time ionospheric variations.

15. SUBJECT TERMS
Theoretical modeling
Empirical modeling
Ionospheric data analysis

16. SECURITY CLASSIFICATION OF:			17. LIMITATION OF ABSTRACT	18. NUMBER OF PAGES	19a. NAME OF RESPONSIBLE PERSON
a. REPORT	b. ABSTRACT	c. THIS PAGE			Peter Sultan, AFRL/VSBP
UNCL	UNCL	UNCL	UNL		19b. TELEPHONE NUMBER *(Include area code)* (781) 377-1309

TABLE OF CONTENTS

Illustrations

Figure 10. A comparison of GTIM values of O^+ density with measurements taken at the Arecibo, PR, ISR facility during April 1995, at four selected Local Times (1900LT, 2200LT, 0100LT, 0400LT). The lines correspond to measurements near the target local times from successive nights, while the symbols are the model estimates, seen to be high in the topside.

Figure 11. As in Figure 10, but showing a comparison of observed and GTIM values of H^+ densities.

Figure 12. The results of a GTIM-based simulation of a geomagnetic disturbance of April 1985. The top panel shows the history of **E x B** vertical drifts, with the dotted line showing the climatological drifts for the period, and the dashed line the disturbance vertical drifts (based on a USU model, and historical AE indices). The middle panel shows contours of variations in Nmax relative to the quiet-time values over a three-day period beginning the day prior to storm onset. Contours are spaced at %10 intervals, positive phases being solid lines, negative phases, dotted lines. The bottom panel shows the same relative deviations but for the three subsequent days-relaxation to pre-storm conditions is evident.

Figure 13. As for Figure 12, but based on a simulation that includes both disturbance drift effects **and** thermospheric effects. Negative phases becomes dominant in addition to a much longer relaxation time.

Figure 14. Longitudinal variations in DMSP F10 in situ density measurements. Six panels denote month and longitude-averaged passes in six longitude sectors for November 1991. The solid line denotes 2100LT data, the dotted line, 0900LT data. The morphology of these density slices shows a marked variation.

Figure 15. Four panels showing density-magnetic latitude variations of O^+ as measured aboard DMSP, for March, June, Spetember and December 1991. Values are month and longitudinally averaged, Evening sector averages are solid lines, morning sector, dotted lines.

Figure 16. As for Figure 15, except the O^+ densities are those derived from the multiple ion GTIM. Evening sector values are plus symbols, morning sector values are squares. A good degree of agreement exists with the observations.

Figure 17. foF2 observations from half a dozen ionosonde stations in the Asian region, for the period 20-24 November, 1961. The solid line in each panel denotes the monthly median diurnal variation, and thus lower ("dropout") values on the 24th are highlighted. Time histories of 3-hourly Kp indices are included along the bottom of each panel.

Figure 18. Variations in TEC, over Hamilton, MA, on May 5 and 6, 1980, plotted sequentially (top panel) and in parallel (bottom panel). A massive dropout is evident.

1. INTRODUCTION

Theoretical models are an important tool in studies of any given environment, as they outline the level to which the physical situation is understood. That is, they help us to answer the question "Does what we see make sense?". Empirical models can also be very useful. They provide a summary of what is observed and/or known about a given situation and typically do so on a short timescale that may well be a factor in an applications-oriented environment. The third, and essential, task in any type of study is data analysis. Especially in the modern era, large amounts of observations can be made rapidly available in real-time, and large historical archives are easily accessed on CDROM. To respond to potentially information-rich environments in a timely and useful fashion, one needs

- the ability to describe the climatology and normal variations of the monitored quantities

- the means to interpret and respond to real-time data, with data-filtering wherever appropriate

- the ability to study large databases and search for new features or behaviors that feed back to theoretical models or that lead to new empirical models.

In this report, we report on a number of ionospheric studies involving variously theoretical models, empirical models, and data analyses. All are ultimately geared towards Air Force objectives of monitoring and specification of the ionospheric environment. There is much overlap between these studies wherein individual projects of one type are being developed in parallel with those of another type. The next three sections of this report outline work performed at Boston University over the last year and a half in each area, but there will be frequent cross-references within the text in order to highlight the parallel nature of the studies.

2. THEORETICAL IONOSPHERIC MODELING

The Air Force Research Laboratories' Global Theoretical Ionospheric Model (hereafter, GTIM) has for many years provided a realiable and realistic description of F region conditions, especially at low latitudes, as originally demonstrated by Anderson (1973a, 1973b) and more recently reviewed by Anderson et al. (1996). Since that time, the formalism developed by Anderson has been extended in order to provide ion density solutions for the light ions, H^+ and He^+. This multiple-ion GTIM is the basis for a number of theoretical modeling studies performed at Boston University. The GTIM has some important advantages over other first-principles models, namely:

- unlike FLIP (Richards and Torr, 1996) and the TDIM (Schunk and Sojka, 1996), equatorial electrodynamics are included, facilitating low-latitude studies

- unlike the TIME-GCM (Roble, 1996), the altitudes modeled are limited only by the number of fieldlines included in the simulation, enabling a full specification of the topside ion densities

- unlike the Sheffield Model/CTIP (Millward et al., 1996), the GTIM has been run using a dense grid of fieldlines at low latitudes with a strong history of validation studies, and the effects of electric field variations on the modeled F region equatorial anomaly have been well-described.

2.1 Light Ion Morphology

The ionospheric specification model, PIM (Daniell et al. 1995) was based in large part on a grid of runs of the F-region GTIM, covering a range of longitudes, seasons, and levels of solar and magnetic activity (where an individual run refers to a large range of magnetic fieldlines for adequate altitude-latitude coverage). To accomplish the same goal using the

multiple ion GTIM, a further grid of models would be required. In parallel with this large grid of model runs, a series of display tools has been developed in order to investigate and eventually describe the morphology of light ions within the GTIM.

To define the morphology of light ions, one needs to both describe the nature of the variations as well as quantifying each variation. One should also compare relative densities of the ions, to define the regions in which each ion is dominant. Let us then define some important parameters with respect to light ion densities, and then display some examples of the results. The full morphology of light ions is still under investigation.

-the first is the (traditional) transition height, this being the altitude at which the H^+ density equals the O^+ density. This ranges from around 500km to 2000km, typically, with local time and solar flux being the dominant influences.

-the second is the H^+ density. Observations suggest that this is not a highly variable quantity overall, that the profile becomes quite slowly varying with altitude (mirroring the neutral H density), and that seasonal and local time variations are not large.

- the third is the He^+ density, a quantity about which little is known a priori from observations. Here, we will examine the nature of the variations as described by the GTIM.

- finally, we include another altitude, this being the height at which the He^+ ion fraction first attains a pre-set value. A value of 0.5 would correspond to an equivalent transition height at which He^+ dominates, but this has proved to be not a frequent occurrence and thus smaller values are generally preferred.

Figure 1 summarizes the results obtained for the O^+-H^+ transition height at solar maximum conditions, at a longitude of $300°E$. There are six panels, corresponding to the even months of the 1991. Each shows the Local Time and (magnetic) latitude variations of the transition height. There is a reasoanble degree of commonality in the variations of

transition height at the different times of year, there being lower values at night, especially pre-dawn, with higher values in the afternoon sector in the equatorial region (corresponding to broad and high O^+ distributions at solar maximum).

Figure 2 shows some of the variations of H^+ densities obtained in the GTIM. In this case, results for February 1991 at a longitude of $300°E$ are presented, with each panel showing the density variations at a selected latitude against local time and altitude. What this figure and a series of other comparisons has shown is that the latitudinal variations of H^+ are typically small, and that Local Time variations are usually small, except around sunrise and sunset when the profiles become even flatter in the upper regions.

In Figure 3, some results for He^+ ion densities are shown in the same format as Figure 2. In this case, the results were obtained for June 1991 conditions. The results show greater variations in all of altitude, latitude and Local Time than were seen in the H^+ results and thus more care will ultimately be required to fully describe the model He^+ ion density variations.

Figure 4 shows the variations in the He^+ ion transition height (defined above), based on an ionization fraction of 0.3. This figure is in the same format as Figure 1, with one panel per month (of the solar maximum year, 1991), showing contours of transition heights against Local Time and (magnetic) latitude. The variations are seen to be quite complex, in addition to there being a number of situations where the ionization fraction is never reached (seen in the blank areas of the middle panels of Figure 4). Howewer, we can also consider the variations based on a fraction of 0.5 (meaning He^+ is the dominant ion), and these results are presented in Figure 5. What is evident here is that there is layering in He^+ ions, and that where there is a majority of He^+ is in the near (F region) topside (at higher altitudes the relative scale heights result in H^+ becoming more dominant). This is consistent with the solar minimum observations of Gonzalez and Sulzer (1996).

Figure 1.

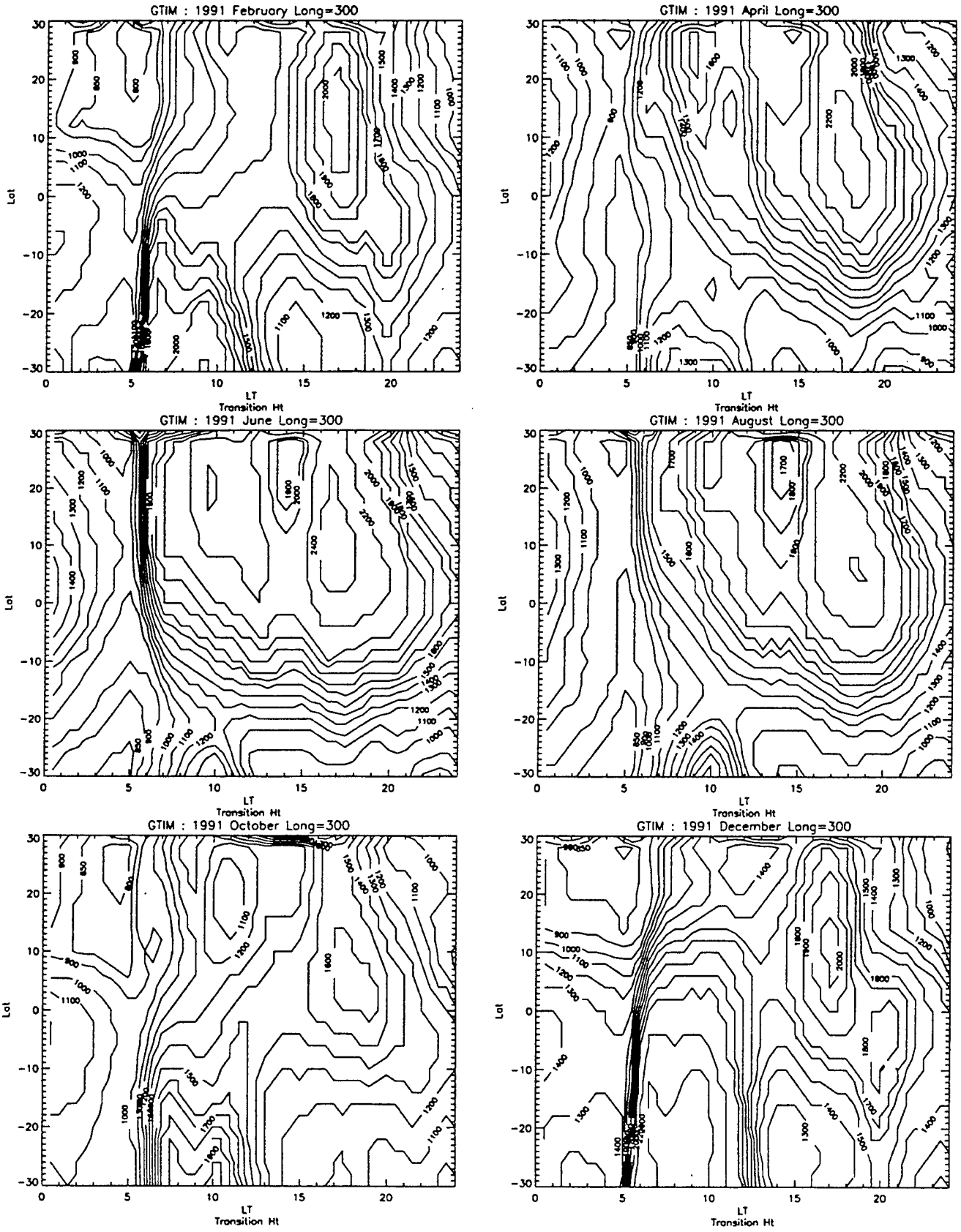
GTIM : 1991 February Long=300
GTIM : 1991 April Long=300
GTIM : 1991 June Long=300
GTIM : 1991 August Long=300
GTIM : 1991 October Long=300
GTIM : 1991 December Long=300
Lat
LT
Transition Ht

Figure 2.

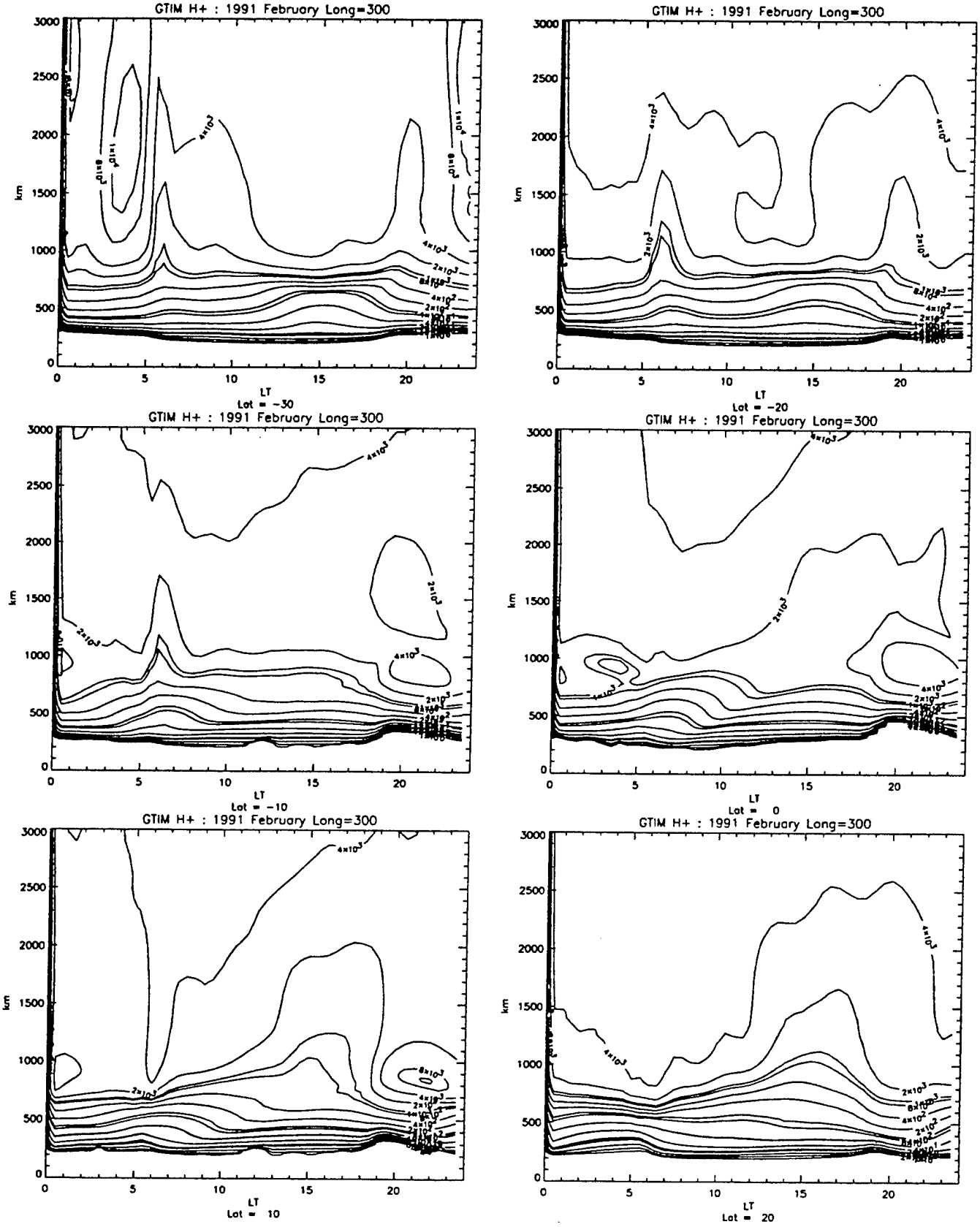
GTIM H+ : 1991 February Long=300
km
LT
Lat = -30
GTIM H+ : 1991 February Long=300
km
LT
Lat = -20
GTIM H+ : 1991 February Long=300
km
LT
Lat = -10
GTIM H+ : 1991 February Long=300
km
LT
Lat = 0
GTIM H+ : 1991 February Long=300
km
LT
Lat = 10
GTIM H+ : 1991 February Long=300
km
LT
Lat = 20

Figure 3.

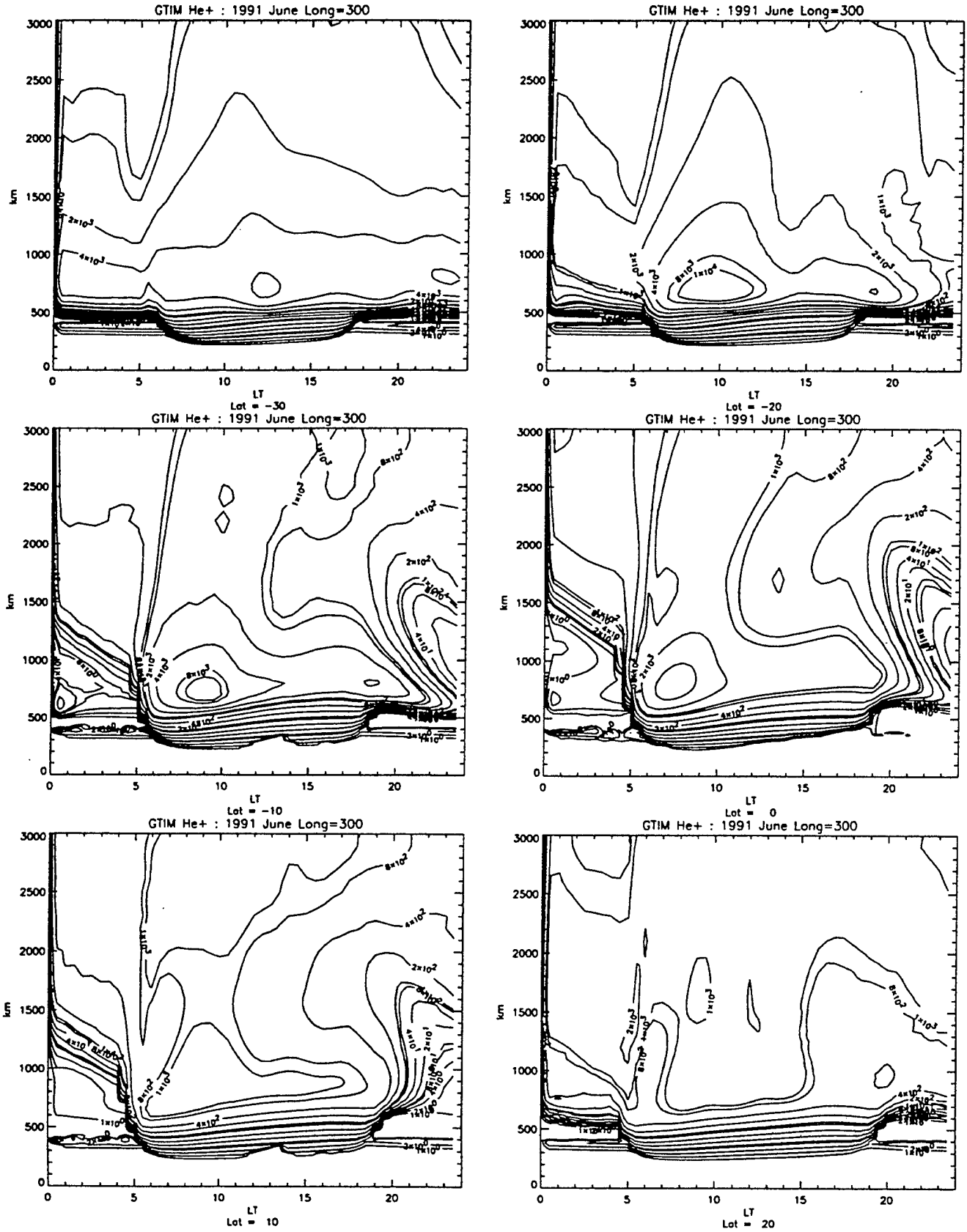
GTIM He+ : 1991 June Long=300
km
LT
Lat = -30
GTIM He+ : 1991 June Long=300
Lat = -20
GTIM He+ : 1991 June Long=300
Lat = -10
GTIM He+ : 1991 June Long=300
Lat = 0
GTIM He+ : 1991 June Long=300
Lat = 10
GTIM He+ : 1991 June Long=300
Lat = 20

Figure 4.

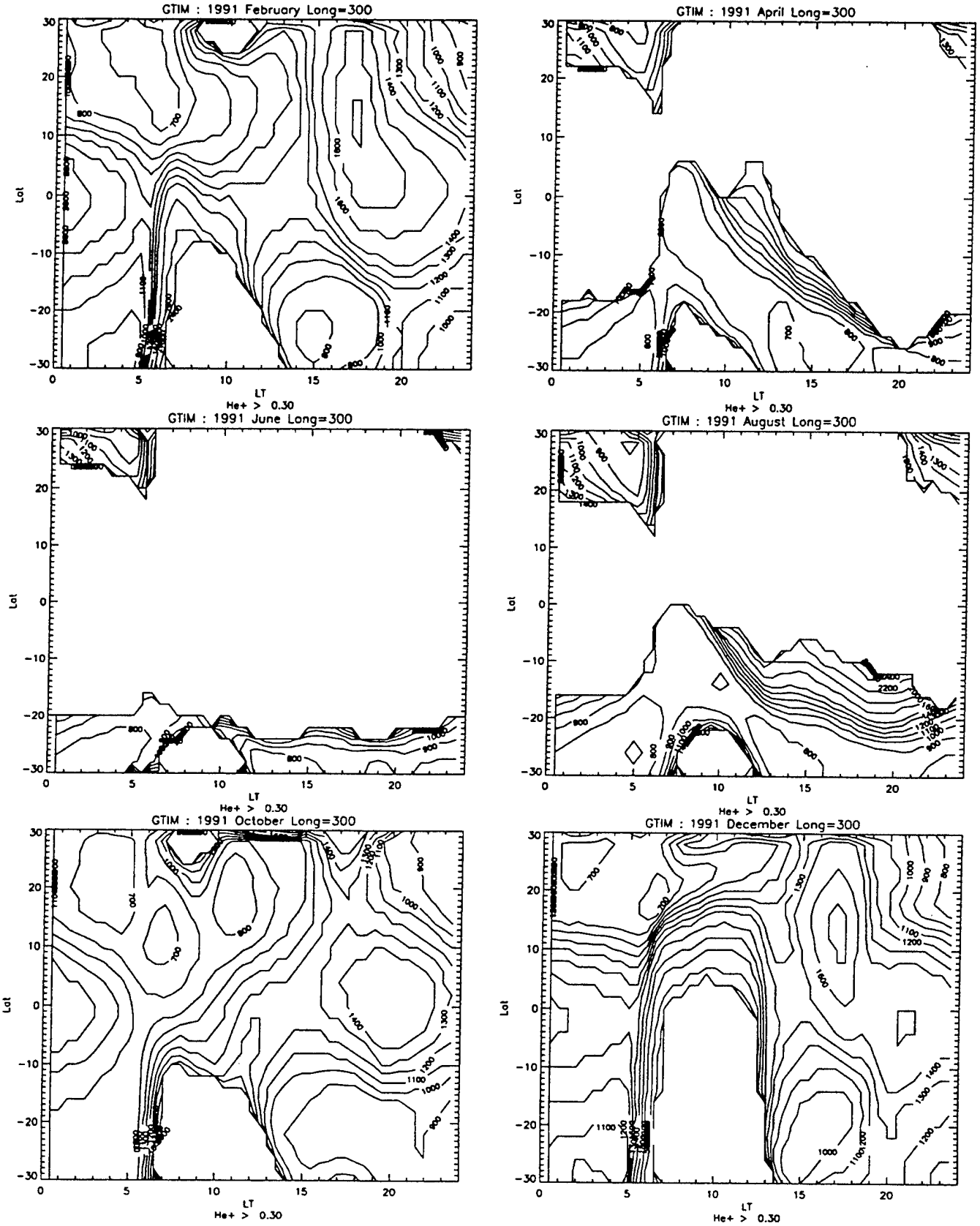
GTIM : 1991 February Long=300
GTIM : 1991 April Long=300
GTIM : 1991 June Long=300
GTIM : 1991 August Long=300
GTIM : 1991 October Long=300
GTIM : 1991 December Long=300
Lat
LT
He+ > 0.30

Figure 5.

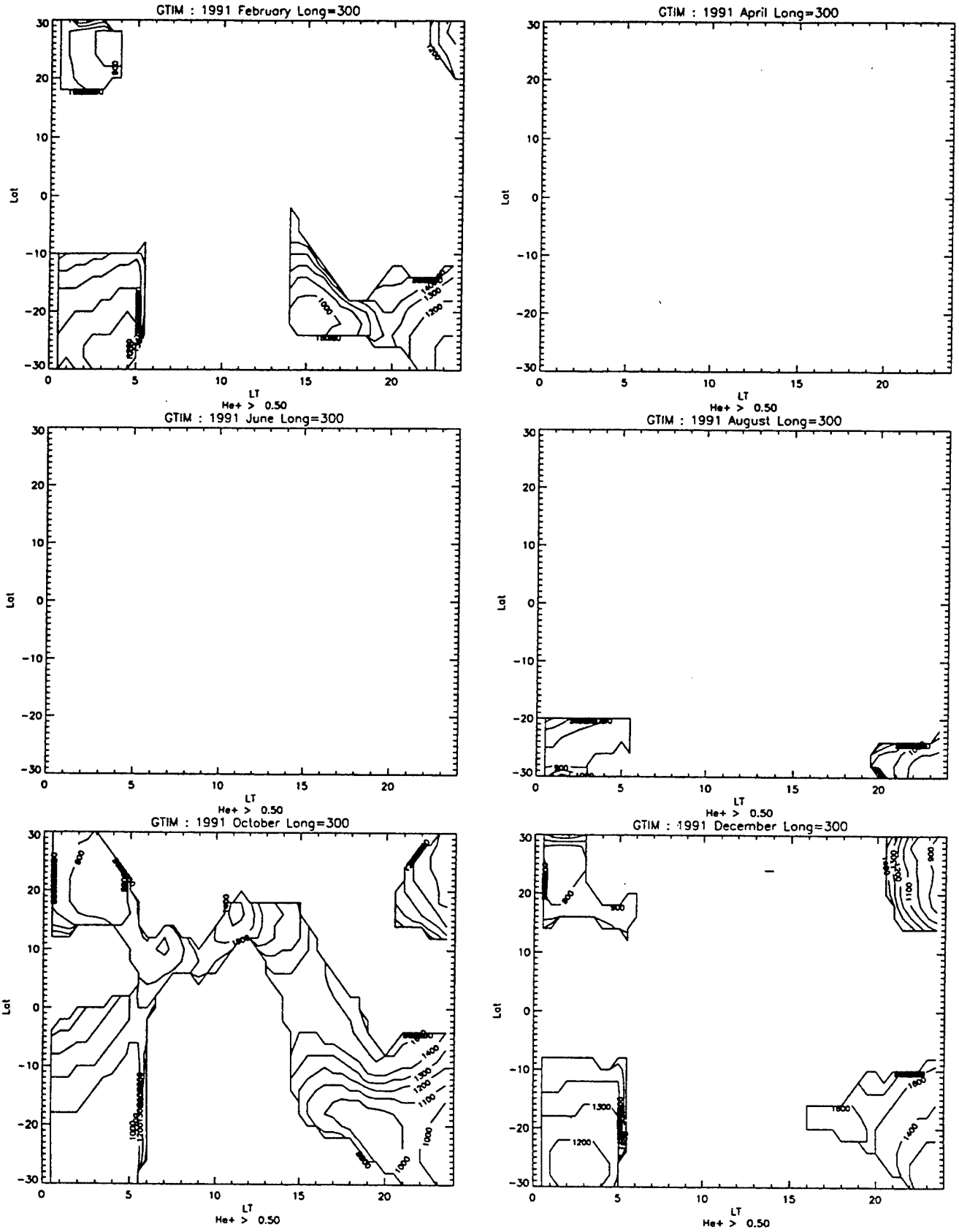
GTIM : 1991 February Long=300
GTIM : 1991 April Long=300
GTIM : 1991 June Long=300
GTIM : 1991 August Long=300
GTIM : 1991 October Long=300
GTIM : 1991 December Long=300
Lat
LT
He+ > 0.50

2.2 Model Validation

A crucial component of theoretical model development is validation of the model predictions against actual observations. In the ionospheric environment, observations are relatively sparse, and the primary assumption in the use of a specification model is that the spatial and temporal gaps between measurements can be filled in with model predictions; this is reliant on the model being able to explain the existing observations and containing all the necessary physics. In the plasmasphere, the sampling of data is far more sparse and the reliance on a model is commensurately greater. However, one ameliorating factor is that the dynamic range of the variations of light ion densities in the plasmasphere (where they dominate) is somewhat less than O^+ variations in the F region. This has also been the case in the GTIM results seen thus far, and as demonstrated in the example in the previous section.

We first consider a grid of model runs designed to validate the F-region specification in the new GTIM; we have taken 1991 and 1994 as representative years of solar maximum and solar minimum respectively. Next, a large range of fieldlines was included in simulations at sample longitudes, and for every two months in each year. Let us first examine the Local Time and latitude variations of Nmax and Hmax within the multiple-ion GTIM. Figure 6 and 7 show the contours of Nmax and Hmax respectively, obtained in the GTIM for each two months of the solar maximum year, 1991, at 300°E longitude. Fieldlines out to L=3.03 were included in these runs to extend the latitude range to greater than 50° magnetic. It is seen in Figure 6 that the equatorial anomaly is well-developed and shows a maximum mnagnitude and extent around the equinoctial months. Correspondingly the equatorial maximum heights are greatest in the equinoctial months, as seen in Figure 7, while heights at middle latitudes are lower and more slowly-varying. The validation of GTIM topside ion densities at solar maximum is presented in Section 2.4, satellite signatures.

Figure 6.

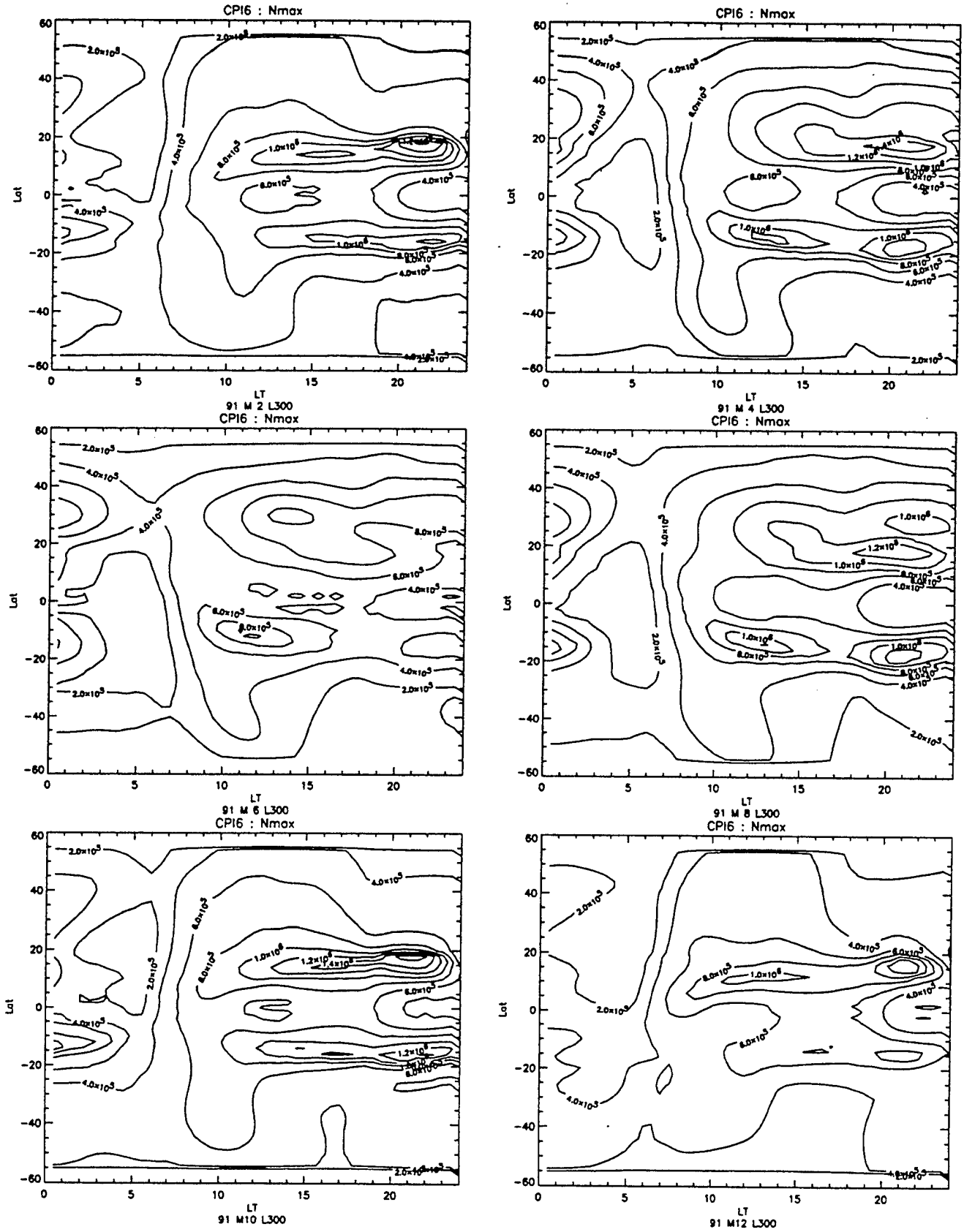
CPI6 : Nmax
Lat
LT
91 M 2 L300
CPI6 : Nmax
Lat
LT
91 M 4 L300
CPI6 : Nmax
Lat
LT
91 M 6 L300
CPI6 : Nmax
Lat
LT
91 M 8 L300
CPI6 : Nmax
Lat
LT
91 M10 L300
CPI6 : Nmax
Lat
LT
91 M12 L300

Figure 7.

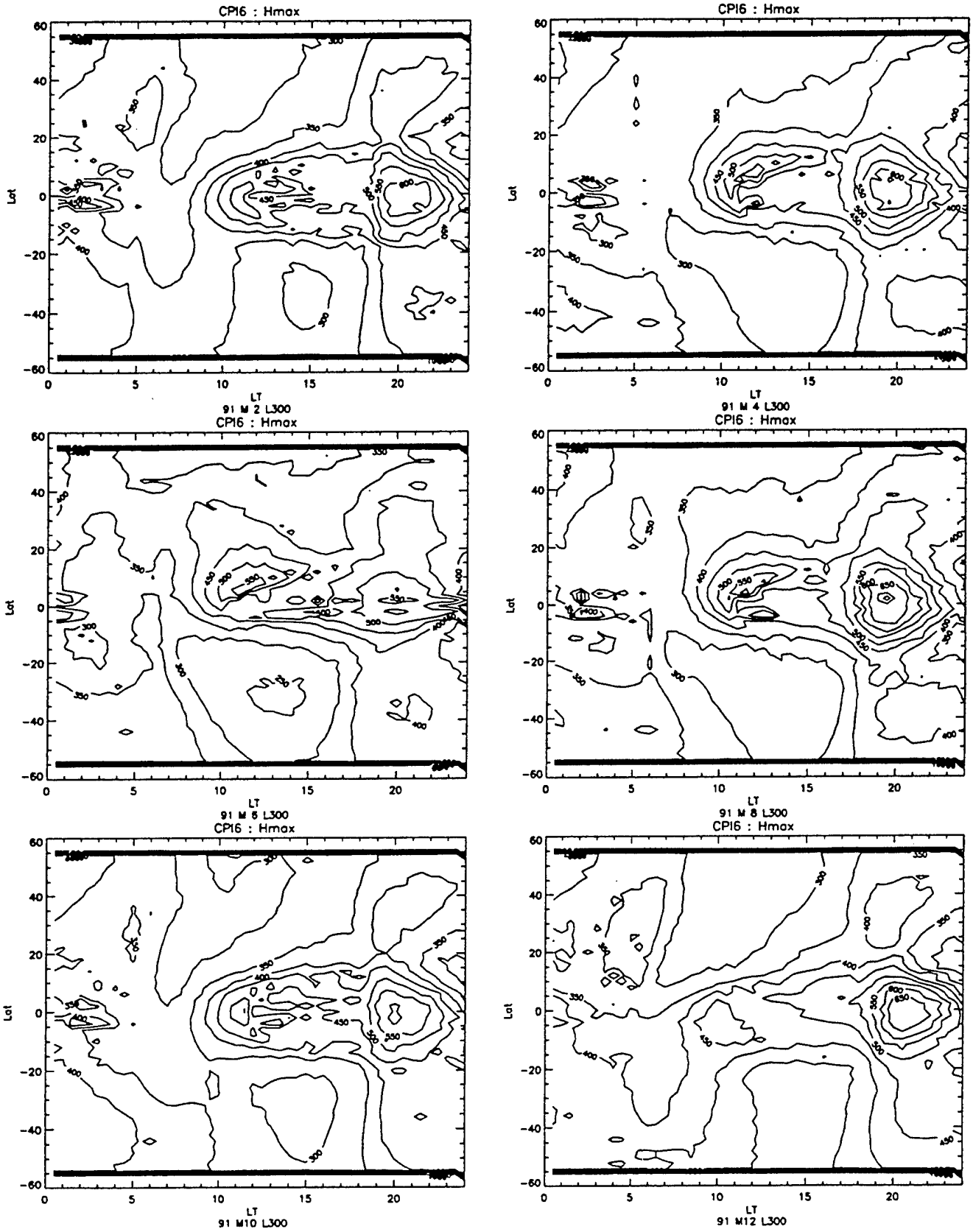
CPI6 : Hmax
Lat
LT
91 M 2 L300
CPI6 : Hmax
Lat
LT
91 M 4 L300
CPI6 : Hmax
Lat
LT
91 M 6 L300
CPI6 : Hmax
Lat
LT
91 M 8 L300
CPI6 : Hmax
Lat
LT
91 M10 L300
CPI6 : Hmax
Lat
LT
91 M12 L300

Figure 8.

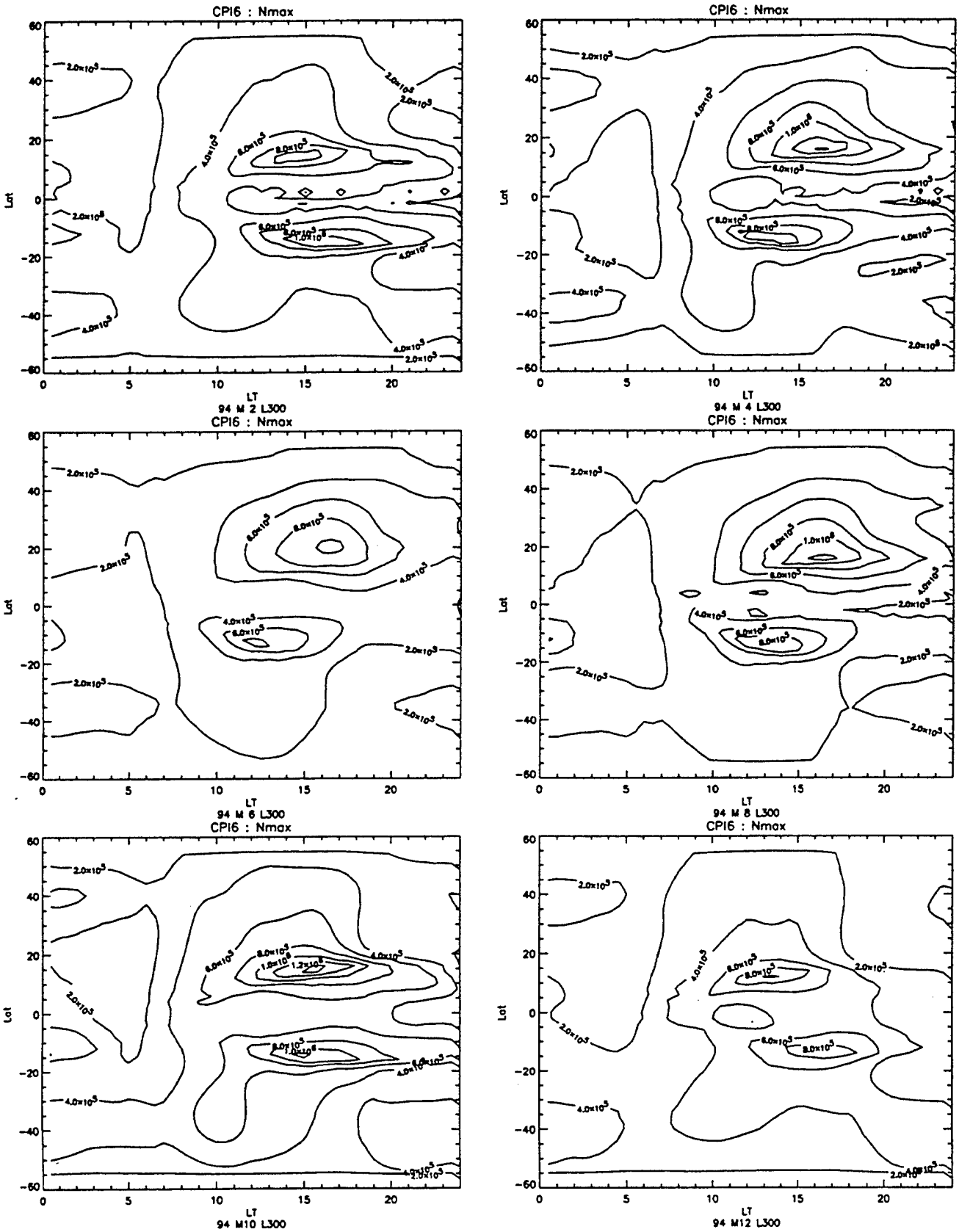
CPI6 : Nmax
Lat
LT
94 M 2 L300
CPI6 : Nmax
Lat
LT
94 M 4 L300
CPI6 : Nmax
Lat
LT
94 M 6 L300
CPI6 : Nmax
Lat
LT
94 M 8 L300
CPI6 : Nmax
Lat
LT
94 M10 L300
CPI6 : Nmax
Lat
LT
94 M12 L300

Figure 9.

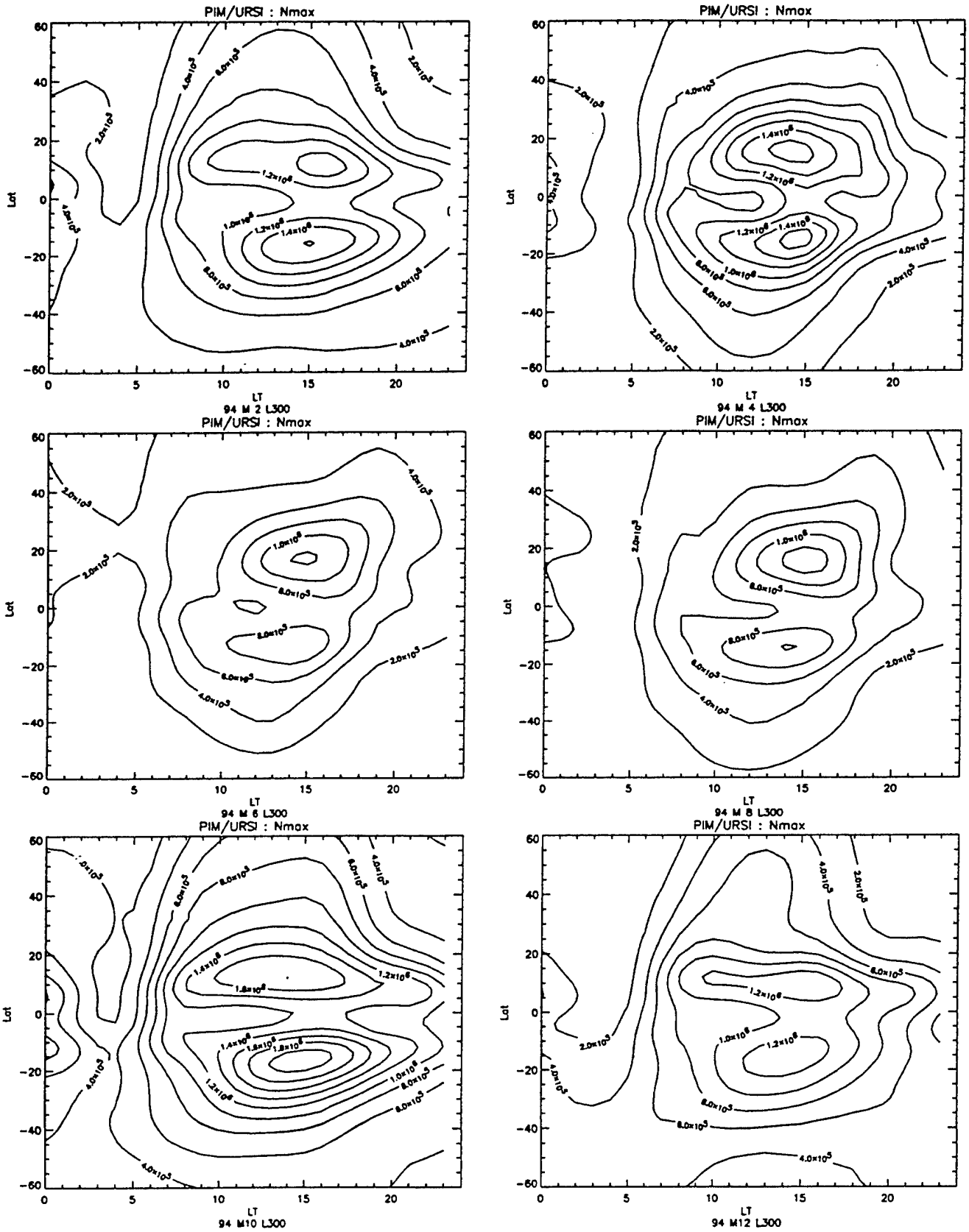
PIM/URSI : Nmax
Lat
LT
94 M 2 L300
PIM/URSI : Nmax
Lat
LT
94 M 4 L300
PIM/URSI : Nmax
Lat
LT
94 M 6 L300
PIM/URSI : Nmax
Lat
LT
94 M 8 L300
PIM/URSI : Nmax
Lat
LT
94 M10 L300
PIM/URSI : Nmax
Lat
LT
94 M12 L300

Figure 10.

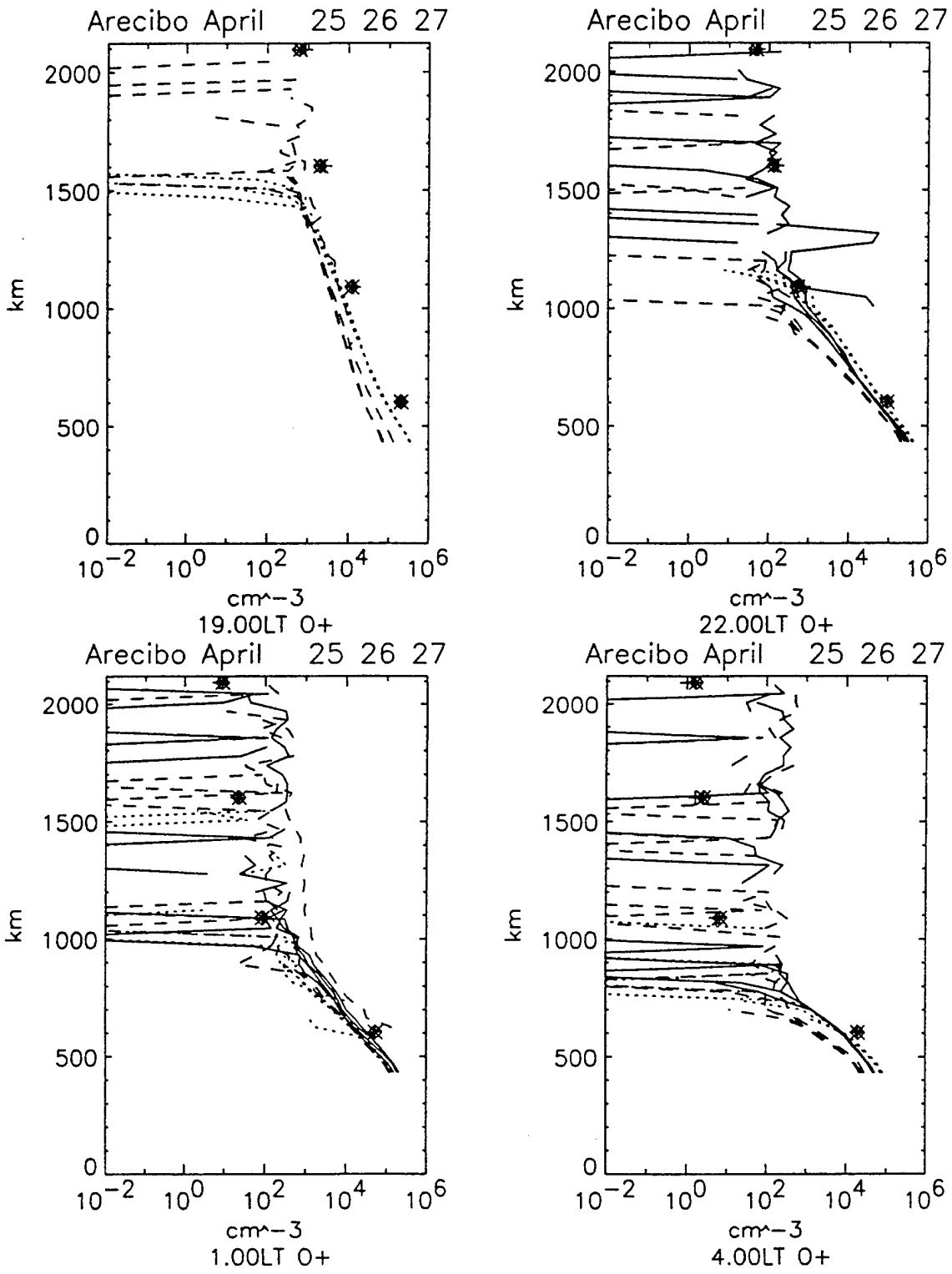
Arecibo April 25 26 27
2000
1500
1000
500
0
km
10^{-2} 10^{0} 10^{2} 10^{4} 10^{6}
cm^-3
19.00LT O+
Arecibo April 25 26 27
22.00LT O+
Arecibo April 25 26 27
1.00LT O+
Arecibo April 25 26 27
4.00LT O+

Figure 11.

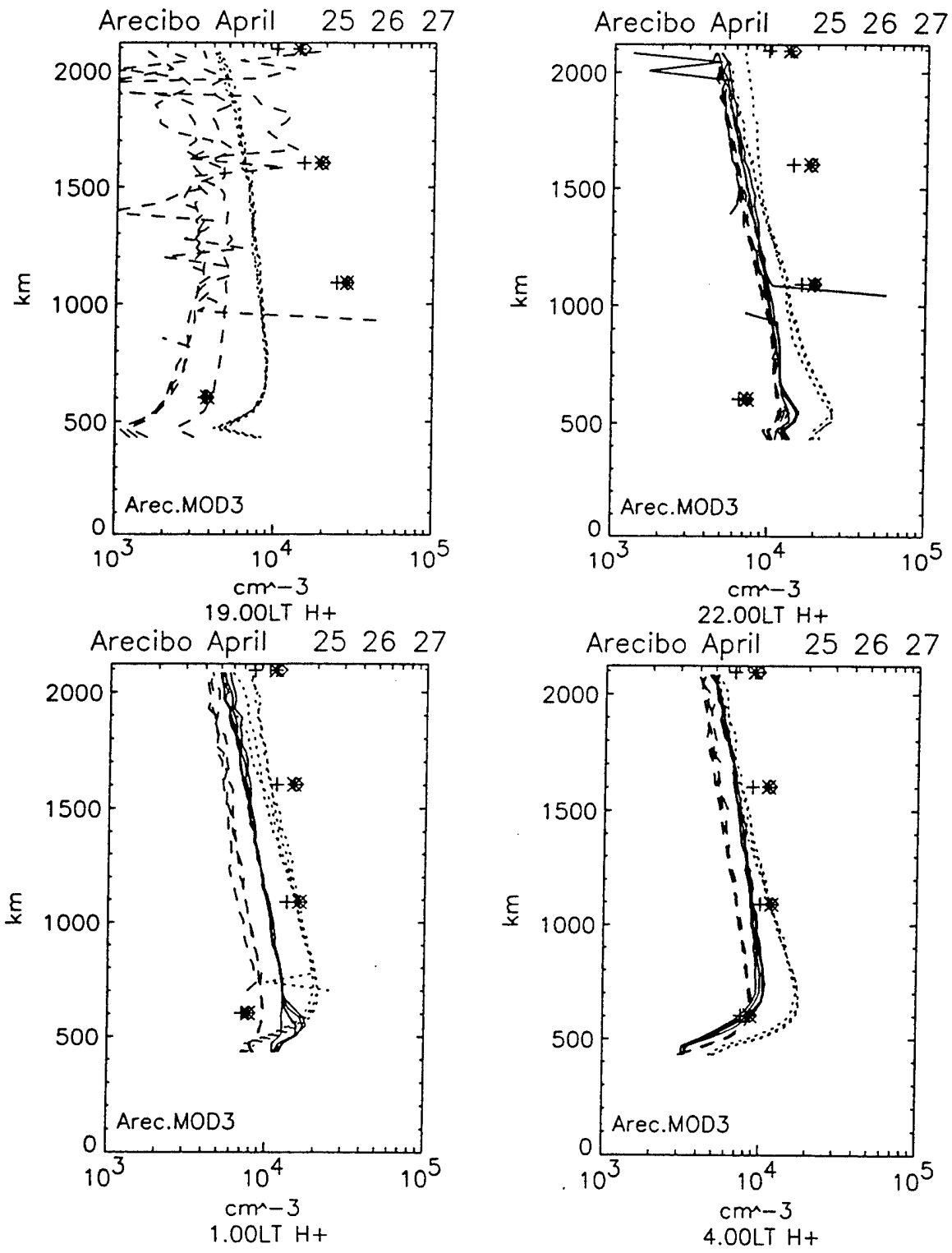
Arecibo April 25 26 27
2000
1500
1000
500
0
km
Arec.MOD3
10^3
10^4
10^5
cm^-3
19.00LT H+
Arecibo April 25 26 27
2000
1500
1000
500
0
km
Arec.MOD3
10^3
10^4
10^5
cm^-3
22.00LT H+
Arecibo April 25 26 27
2000
1500
1000
500
0
km
Arec.MOD3
10^3
10^4
10^5
cm^-3
1.00LT H+
Arecibo April 25 26 27
2000
1500
1000
500
0
km
Arec.MOD3
10^3
10^4
10^5
cm^-3
4.00LT H+

At solar minimum, however, a discrepancy was revealed. For example, the Nmax variations in the GTIM is shown in Figure 8 in the style of Figure 6 but for the solar minimum year, 1994. A contrast of these results with those based on the URSI coefficients that are shown in Figure 9 shows that the GTIM Nmax results are systematically low. While it is true that the URSI coefficients at low latitudes should not be treated as much more than a guide, the differences are significant. That the discrepancy extends into the topside has been demonstrated by comparisons of GTIM results with variously, ISR data from Arecibo, DMSP observations taken in 1994 on F12, and solar minimum TOPEX vertical TEC measurements that reveal the GTIM O^+ topside results (and correspondingly, the H^+ densities, as charge exchange is the primary source of H^+) to be systematically high. The Arecibo comparisons, shown in Figures 10 and 11 (for O^+ and H^+ respectively, at four selected Local Times, the lines denoting ISR observations, while the symbols are densities from the GTIM) demonstrate this effect quite clearly; the GTIM O^+ and H^+ topside densities are higher than the observed values.

2.3 Dynamo Model Driving

The GTIM is an established model at low latitudes that has been shown to provide a good description of the equatorial F region when **ExB** vertical drifts are known. As such, it is a good basis from which to attempt to model the ionospheric effects of (geomagnetic) disturbances at low latitudes. The motivation for the study came from a newly-developed empirical description of disturbance vertical drifts from Utah State University (hereafter, USU) (Scherliess and Fejer, 1997; Fejer and Scherliess, 1997) driven by the magnetic AE index. A further implication in terms of this contract work is to investigate the nature of ion density changes to impulsive events (i.e. storms), as this will provide constraints on the nature of real-time adjustments that will be of concern when the multiple-ion GTIM begets the next generation of PRISM model.

An adaptation of the GTIM was thus developed, performing normally for a number of days using quiet-time or climatological drifts to allow convergence of the ion densities (filling of the plasmasphere is not a concern here as all the fieldlines considered in these runs are low L values). At storm onset the disturbance drifts are used at each subsequent time step until the drifts have again relaxed to the quiet-time pattern. The model is then run for three additional days to be able to judge the relaxation time for the modeled ionospheric reponse. Typically the modeled response presented is in three-day blocks corresponding to "during" the storm and "after" the storm, concentrating on the difference between the modeled ionosphere and the (converged) ionosphere prior to storm onset. At the lowest fieldlines (Mode=2 in GTIM parlance), a slightly different method is used. Normally the GTIM will start off a low fieldline (L=1.026 usually) at a given local time and then terminate the run when the apex altitude reaches a lower limit (physically, the fieldline is then at a low enough altitude that loss will dominate and thus the ions recombine), and coverage at low latitudes is obtained by starting fieldlines at a number of different local times. In this case, we want to pursue all fieldlines over a period of a number of days (if only to simplify the accounting) for these disturbance drift studies, and so the lowest fieldlines are maintained at the lowest altitude (i.e. fixed at the minimum altitude) until a time when upwards convection has again compensated for the net downward movement.

In adapting the GTIM to disturbance modeling, we also enabled thermospheric driving (MSIS and HWM using a storm-time Ap index), in addition to the abovementioned disturbance drift driving. Model runs with and without thermospheric driving can help describe and isolate the thermospheric and drift-based effects.

A sample of disturbance vertical drifts has been provided by colleagues at USU to commence this modeling study. These drift patterns correspond to:

1) a sample of ideal storms; these were based upon a simple "event" in AE (the

parameter that drives the disturbance drift model) a range of onset local times as well as both solar minimum and solar maximum conditions

2) a case study; a storm in April 1985 met the criteria of being far enough back in time to have AE listed, being isolated from neighboring storms, and being large enough to be of some interest (in terms of ionospheric response).

The results for the case study are shown in Figure 12. The top panel of this figure shows the drift history over a three-day period where the dotted line is the quiet-time pattern (repeated each day for clarity) and the dashed line shows the model disturbance drifts. Storm onset is evident in the middle of the first day. The middle panel shows a contour plot in local time (over three days) and magnetic latitude of the changes in Nmax derived using the GTIM with the drifts in the top panel. The changes are plotted as percentage changes in Nmax compared to the quiet-time values, the contours being spaced at 10% change levels, and where dotted lines show negative phase and solid lines show positive phase for clarity. The bottom panel shows the results for the three subsequent days. In this figure, one thus sees

- a strong positive storm phase at low latitudes on the second night
- a smaller negative phase on the following day
- relaxation to quiet conditions by the third day
- some smaller positive and negative phases in the anomaly region on the second day
- little storm response on the day of the storm onset.

The case study storm was then run using both disturbance drift and thermospheric drivers, as described above. The results of this run are shown in Figure 13. What is immediately apparent here is that the thermospheric effects all point to negative storm phases that can strongly mitigate the dynamo-driven positive phases, and that these

Figure 12.

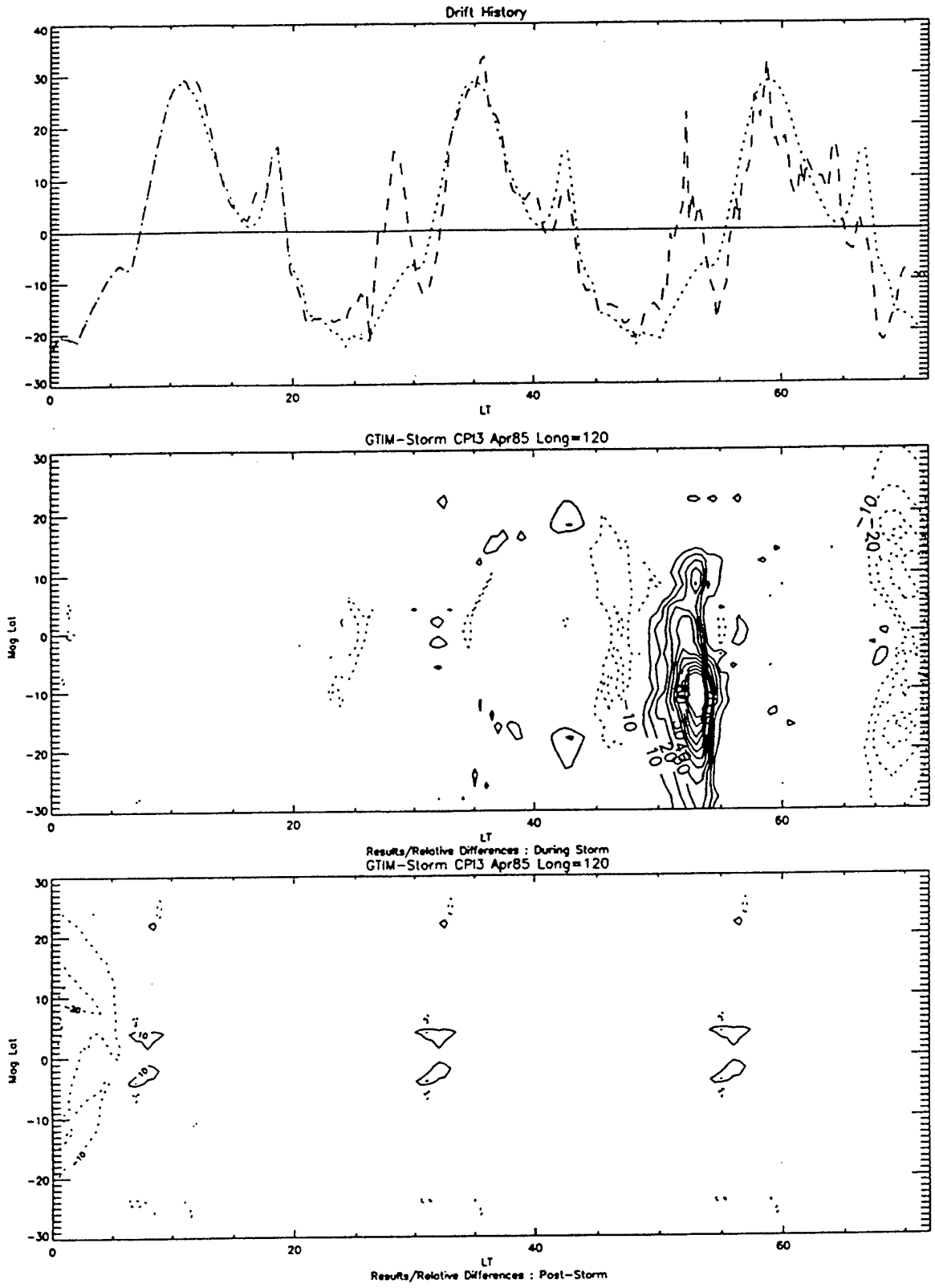
Drift History
LT
GTIM-Storm CP13 Apr85 Long=120
Mag Lat
LT
Results/Relative Differences : During Storm
GTIM-Storm CP13 Apr85 Long=120
Mag Lat
LT
Results/Relative Differences : Post-Storm

Figure 13.

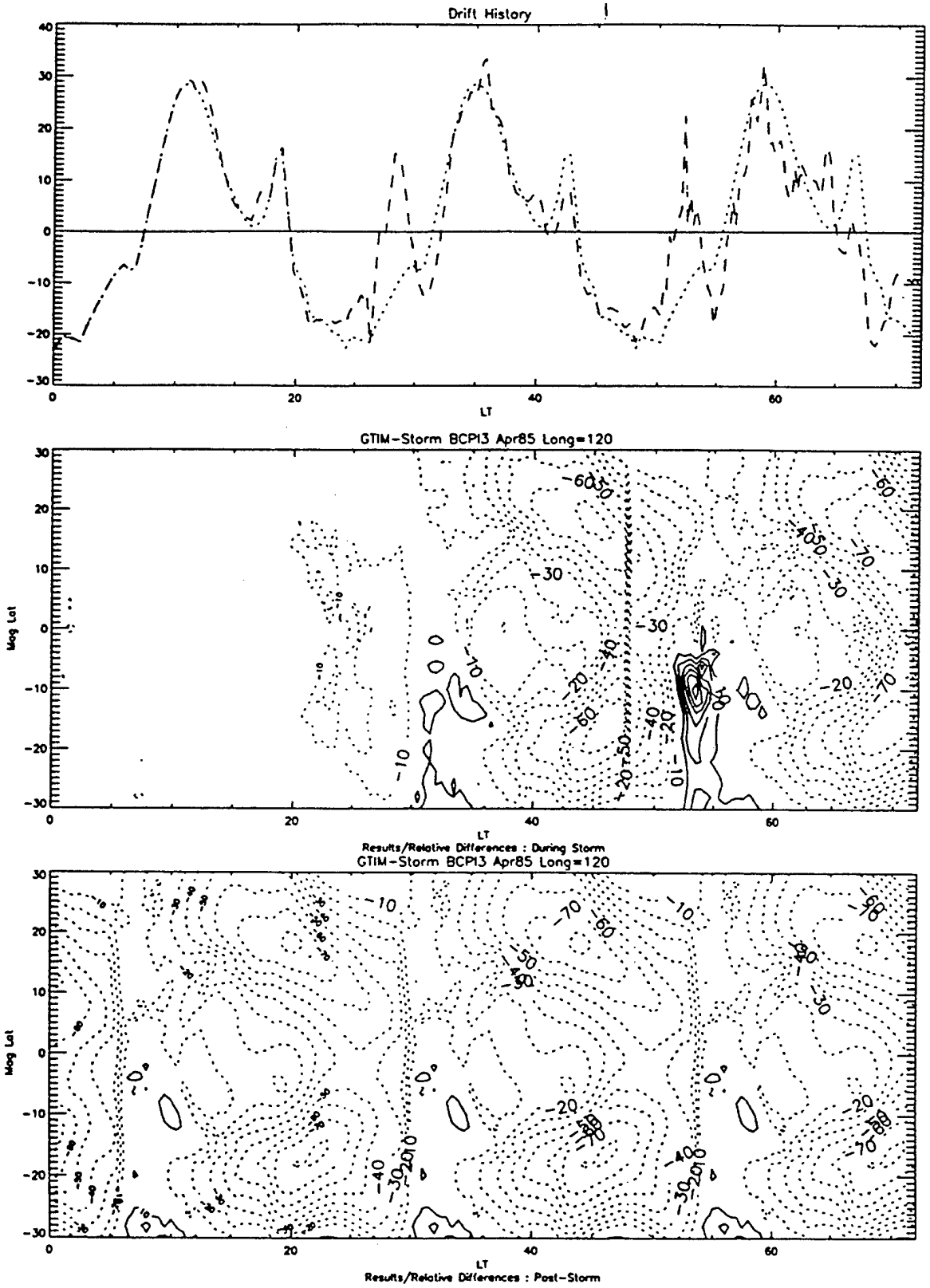
Drift History
LT
GTIM-Storm BCP13 Apr85 Long=120
Mag Lat
LT
Results/Relative Differences : During Storm
GTIM-Storm BCP13 Apr85 Long=120
Mag Lat
LT
Results/Relative Differences : Post-Storm

negative phases can endure for a number of days after the drift effects have returned to normal. This arises because the Ap histories in MSIS and HWM have a longer timescale than does the USU disturbance drift model, reflecting real timescales in the thermosphere and disturbance dynamo.

A number of runs were made on the grid of conditions for "ideal" storms. Some highlights of these ideal storm runs were:

- typically, the commonest response is a nighttime positive phase (additional upward nighttime drifts helping to maintain ionization at night)

- secondary responses are in the anomaly region, and may be positive or negative in phase

- thermospheric effects are almost invariably negative phase

- evening sector onset times provided the larger disturbance drifts and hence the larger ionospheric responses

- solar minimum (percentage) effects are slightly larger in magnitude than solar maximum.

Currently, these dynamo modeling studies are being held in place. In the future, the following tests are envisaged:

- completion of the grid of ideal storms and listing of the dependencies of storm response on various factors

- a closer study of the disturbance modeling to determine why in many cases the modeled storm response takes more than one day after storm onset (this is more apparent in the ideal storm runs)

- collaboration with JPL on a second storm case study, utilizing the GPS-based global

TEC maps to illustrate ionospheric reponse on a larger scale than can be gleaned from the small sample of equatorial ionospheric stations. This latter point is the greatest factor in delaying future work. Best coverage of effects at low latitudes from the JPL network requires that the event come from 1996 or later- while on the other hand, the AE indices driving the USU empirical dynamo drift model take a significant amount of time before becoming available. Further, events from 1996 and on would be all solar minimum and thus should be deferred until the current solar minimum discrepancy with the multiple ion GTIM can be resolved.

2.4 Satellite Signatures

A study of Special Sensor Ion Electron Scintillations (hereafter, SSIES) in situ satellite signatures using the GTIM has been conducted. The goal of this work was to produce a set of numerical calibrations for effective levels of pre-reversal vertical drift and neutral wind based on SSIES density measurements. Grids of GTIM runs were computed over a range of conditions (and independent grids of vertical drift and neutral wind) and the resultant patterns compared to observations. This was to ensure:

- that the model could match the absolute densities observed and span the range of density slices

- that robust parameters could be found using the GTIM density values that relate simply to the levels of both vertical drift and neutral wind.

This latest set of GTIM runs has been based upon a drift model provided by Dr. R. E. Daniell of CPI, Boston, that fully utilizes recently published AE-based drift measurements of Fejer et al. (1995). This model contains a Fourier representation of the annual variations and thus is available at all months with smooth transtions between the characteristic seasonal variations. There is also a smooth longitude variation built into this empirical drift

model.

We refer now to the question of model validation, raised the first of the points listed above. Figure 14 shows O^+ densities as a function of (magnetic) latitude as measured on F10 during March, June, September and December 1991. The lines are monthly averages, and further averaged within 30 degree of 60°E longitude. The solid line reflects the 2100LT pass, the dotted line 0900LT data. Next, Figure 15 shows GTIM O^+ densities for the same four epochs, solar actitivy levels, and longitude, using the same vertical scale. A comparison of the two figures reveals a high degree of correlation. This could be further demonstrated at other months and other longitude sectors. It could also be shown that the range of daily (sector-averaged) values could be spanned by a grid of GTIM runs that include a rnage of neutral wind and vertical drift scalings.

We now consider the effects neutral winds. It was expected that the neutral wind would manifest itself most dramatically in the asymmetry of the in situ density values, and this certainly held true in the GTIM results. Indeed, a simple linear fit was sufficient to describe the numerical relationship between the wind scaling value and the north-south asymmetry (or south-north, in general, whichever is the larger) in the densities; this latter quantity was defined as the ratio of densities averaged over a range of latitudes (15-30 degrees proved to be the most stable range). An average is advantageous as it overcomes a strong dependence of 840km density values on the **daily** solar flux, an effect that has been observed as wellas being reproduced in the GTIM results.

Consider vertical drifts next. The use of a ratio of average (of north and south) anomaly crest density to the equatorial trough density showed a clear and dramatic increase with increasing vertical drift level, although a linear relationship was not sufficient. However, there was another factor to consider in the derivation of effective vertical drifts. This being that there are not always crests in SSIES measurements at 840km, especially at

Figure 14.

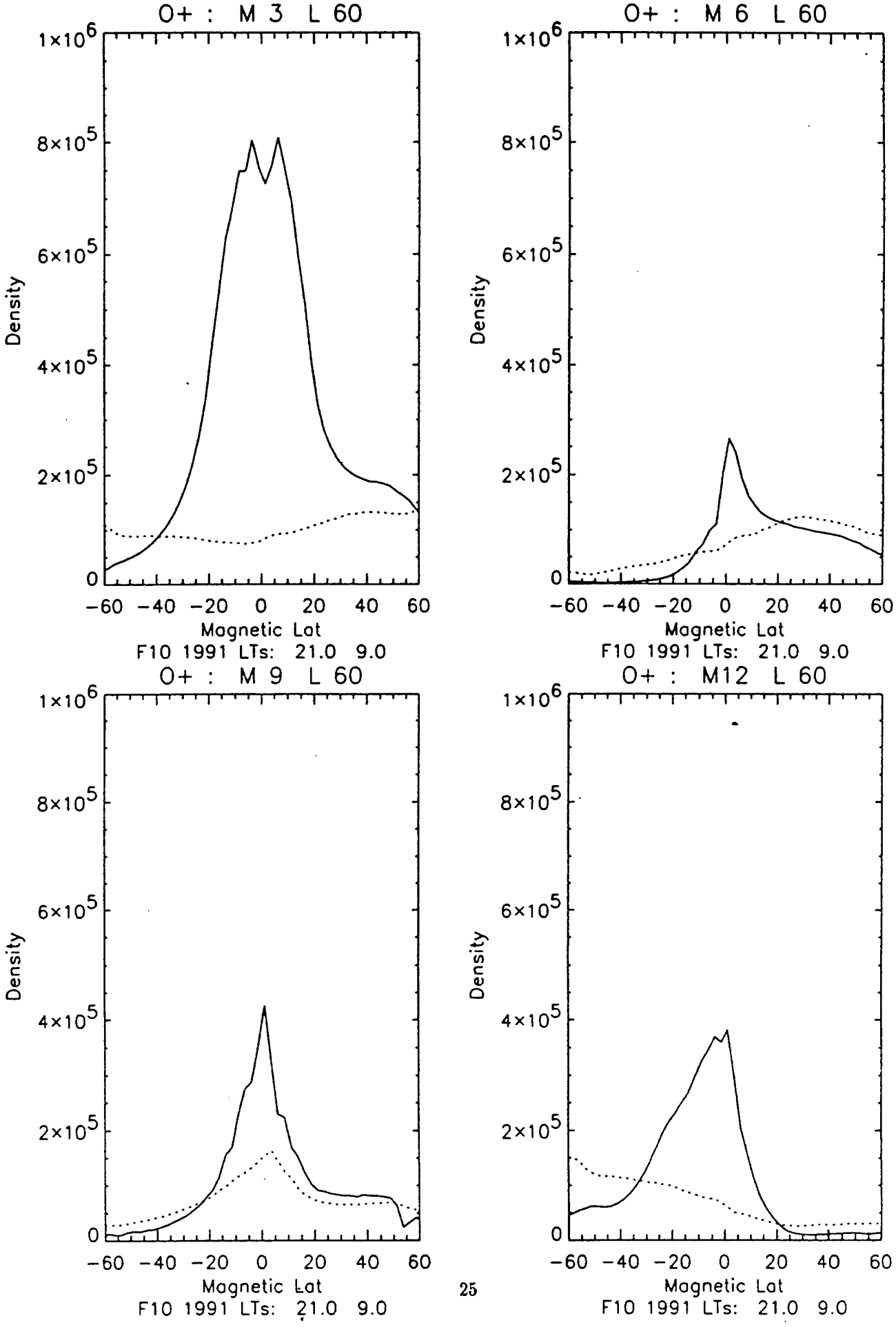
O+ : M 3 L 60
O+ : M 6 L 60
O+ : M 9 L 60
O+ : M12 L 60
Density
1×10^6
8×10^5
6×10^5
4×10^5
2×10^5
0
−60 −40 −20 0 20 40 60
Magnetic Lat
F10 1991 LTs: 21.0 9.0

Figure 15.

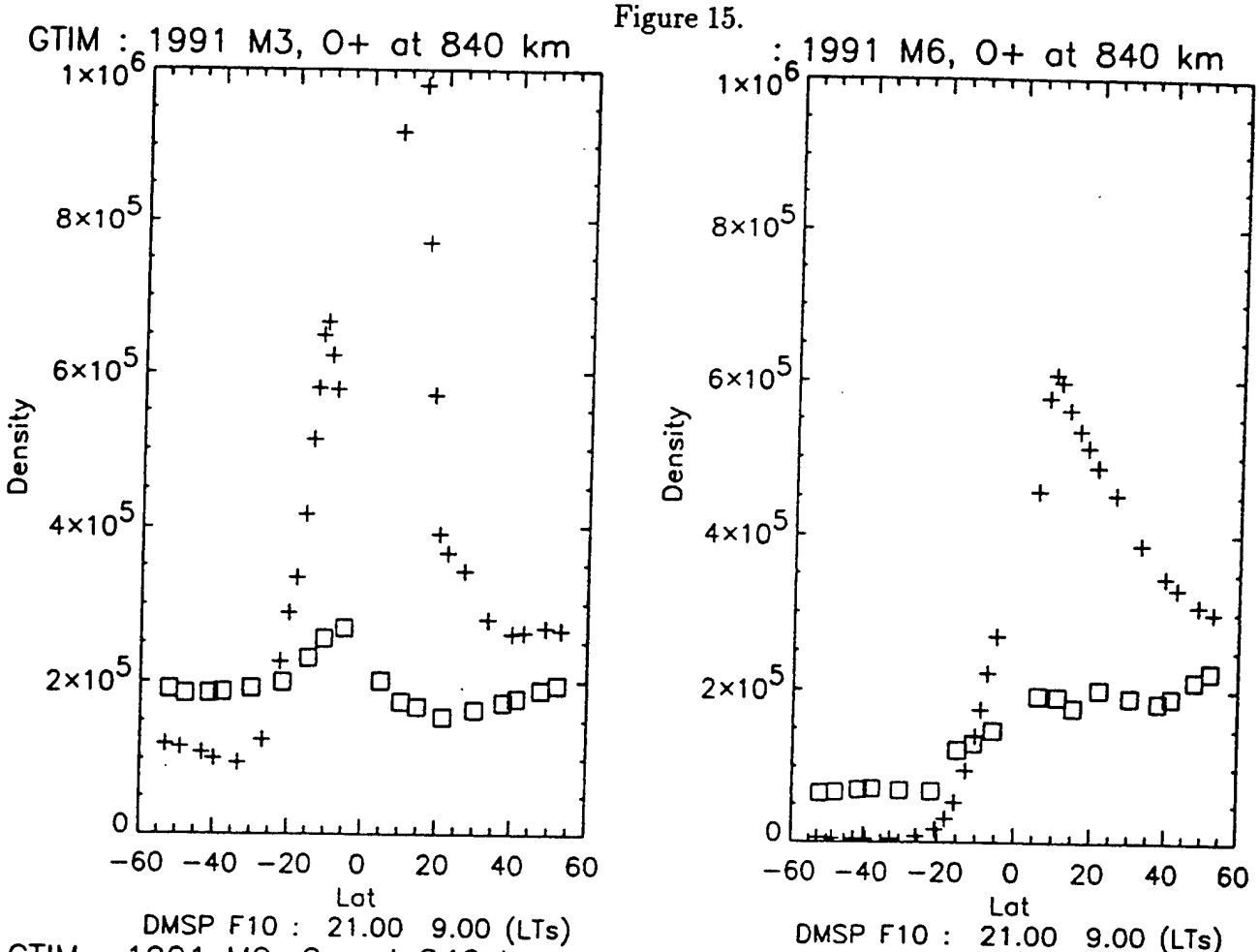
GTIM : 1991 M3, O+ at 840 km
: 1991 M6, O+ at 840 km
Density
1×10^6
8×10^5
6×10^5
4×10^5
2×10^5
0
−60 −40 −20 0 20 40 60
Lat
DMSP F10 : 21.00 9.00 (LTs)

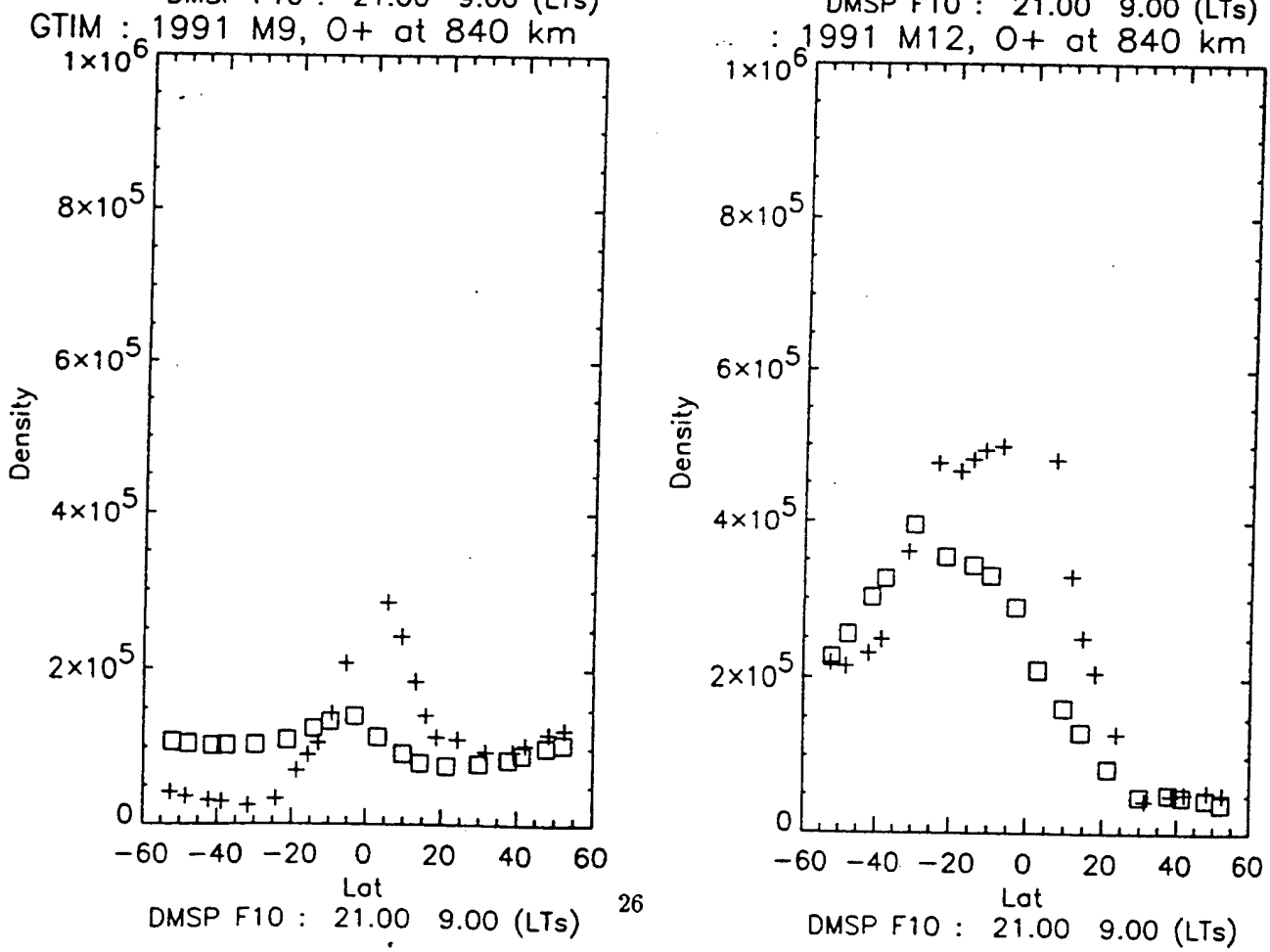
GTIM : 1991 M9, O+ at 840 km
: 1991 M12, O+ at 840 km
Density
1×10^6
8×10^5
6×10^5
4×10^5
2×10^5
0
−60 −40 −20 0 20 40 60
Lat
DMSP F10 : 21.00 9.00 (LTs)

solsticial months when pre-reversal enhancements are typically small. To derive effective drifts at lower drift levels/seasons, a new parameter was defined; this is the ratio of the equatorial density to the average density in the wings (defined at the same latitude ranges as the wing ratios used to derive effective neutral winds).

Robustness in the algorithms has been enhanced via additional grids of GTIM model runs. Initially, the parameters chosen to specify effective wind and drift levels from SSIES density signatures had a good level of robustness built in:

- the use of density ratios as the parameters made the relationships largely robust to daily solar flux variations

- the use of averaged (hemispherically) density ratios for vertical drift derivation made them largely robust to neutral wind variations

- the use of ratios of densities in the (mid-latitude) wings for effective wind derivation made them largely robust to vertical drift variations

- the use of densities at the peak and trough locations rather than at fixed locations (latitudes) made them robust with respect to altitude variations in the vertical drift.

However, the level of robustness can be enhanced. This is because even with a careful choice of parameters, there is some wind-dependence in the calibration of drifts and vice-versa. For example, at the climatological wind value, a slightly different effective drift calibration is derived than at twice the wind value; and not only that the correlation is different depending on whether or not crests exists, but also that a correlation can exist at lower effective drift values when no crests are seen. In a number of comparisons conducted here with SSIES density slices with the GTIM, it is apparent that variations in effective wind and drift values of more than 100% are not infrequent.

For the above reasons, for each month in 1991 (the solar maximum year) the following

grid of models has been run:

- default wind level, a range of vertical drift levels
- zero wind level, a range of vertical drift levels
- double wind level, a range of vertical drift levels
- default drift level, a range of neutral wind levels
- zero drift level, a range of wind levels
- double drift level, a range of wind levels.

Coefficients have been derived using the newest version of the GTIM with the analytic expression for vertical drifts. The procedure for deriving effective wind and drift levels has been written in software and consists of the following steps:

1. Derive the effective wind, W, assuming a default vertical drift. The wind calibration is always linear and is thus more stable as a starting point.

2. Go to the nearest vertical drift calibration for the level of wind derived in Step 1. That is, if $W < 0.5$, use W=0.0, if $W > 1.5$, use W=2.0. If there are crests present, use the ratio of crest to trough, and if not, use the ratio of equator to wings to derive the drift, D.

3. If $D < 0.5$, redo Step 1 using the D=0.0 calibration for winds. If $D > 1.5$, redo Step 1 using the D=2.0 calibration for winds.

4. If the wind, W, derived from Step 3 is significantly different from 1, then derive D again, as per step 2, for the appropriate wind level.

In extreme cases, the results may not be an estimate of W or D, but rather an indication such as $W<0.0$ or $D>2.0$. The practical application of these algorithms at the next solar maximum will reveal whether or not further grids of model runs (to more extreme wind or drift levels) is required. A detailed example of the use of the coefficients

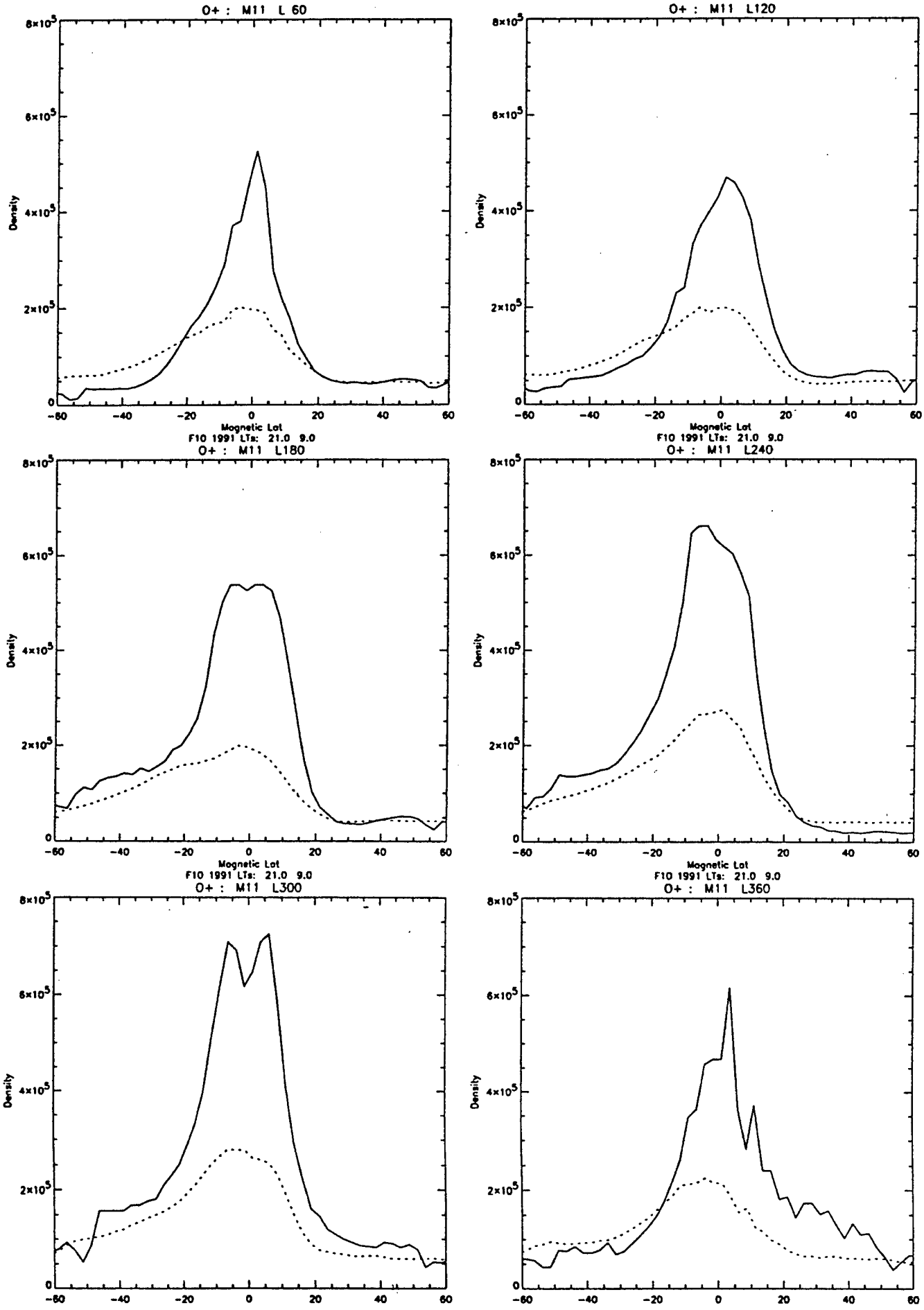
O+ : M11 L 60
O+ : M11 L120
O+ : M11 L180
O+ : M11 L240
O+ : M11 L300
O+ : M11 L360
Density
Magnetic Lat
F10 1991 LTs: 21.0 9.0

was included in quarterly report no. 4 on this contract.

Currently, we are endeavoring to make the solar maximum study more robust in terms of being extended to other longitudes, with the generation of additional model runs and the development of software to define the longitude variations. Longitude variations are certainly apparent in the SSIES observations. Figure 16 shows the data from DMSP F10 plotted using monthly/longitude averages for November 1991, in six different longitude zones (longitude E=60,120,180,240,300,360). Each panel shows the average density versus latitude pattern for the month for O^+ at both 2100LT (solid line) and 0900LT (dotted line) passes and this figure reveals changes in the morphology of the densities due solely to the longitude.

The goal of this latest work is to establish the simplest description of the longitude variations. At worst, the same types of coefficients could be established within each longitude sector. For brevity, however, it would be preferred to simply establish a very similar nature of the correlations at all longitudes, and to account for different longitudes with simple adjustments at the coefficient level. Tests to determine the simplest (and yet realistic) nature of the longitude variations are currently underway.

3. EMPIRICAL IONOSPHERIC MODELING

The work described herein utilizes the work of Fox (1994), wherein a simple, analytic and realistic formalism for electron density profiles was developed. A number of applications of this analytic description have been explored.

3.1 Profile Shapes

This section summarizes recent work performed at Boston University that is geared to providing quick and reliable estimates of slant TEC based on an ionosphere generated from

PIM (Daniell et al., 1995). The issue here is that while PIM provides a ready climatological estimate for ionospheric electron densities within a region (likewise, PRISM attempts to describe "weather" conditions), that the vertical profiles generated on a coordinate grid do not lend themselves to a ready evaluation of TEC along arbitrary lines of sight. What has been performed here is a study of the feasability of one possible solution to this.

The solution contains the following steps:

1. PIM/PRISM generated electron density profiles are fit with analytic functions. These functions are variable scale-height Chapman-layers in both the topside and bottomside, as described in Fox (1994). Each vertical profile fit thusly is summarized by six parameters (two peak, two topside, two bottomside).

2. Each of these six fitted parameters vary smoothly in both location and time, so can at any given time be fit in two dimensions.

3. Electron densities at any location and altitude can be quickly regenerated from fits that are analytic in all dimensions.

4. Slant TECs can be calculated from a ground station by summing electron densities thus regenerated along the slant path.

The results are listed below, according to the step, as listed above.

Step 1- Running and Fitting PIM

The first issue here is what size the grid of PIM profiles should be in order to adequately specify TEC. This depends on two factors:

- the minimum elevation angle that we wish to simulate slant TEC

- the accuracy to which TEC is desired.

A range of model ionospheres has been included in these simulations, to include both middle and low latitudes, and cover various local time domains.

A series of tests established that:

- to simulate elevation angles below 60°, the grid should extend 20° in both latitude and longitude from the "ground station"

- to simulate elevation angles below 30°, the grid should extend 30°

- to simulate elevation angles below 10°, the grid should extend 40°.

The grid spacing in latitude and longitude has been shown in tests to not be an important factor. Over a range of ionospheric locations and conditions and a range of resolutions from 10° in longitude and 4° in latitude to 2° in longitude and 1° in latitude there was no appreciable change in the resultant slant TEC. There simply needs to be sufficient resolution in the grid to define the ionospheric morphology.

The above figures are based upon a desired accuracy of 1% for slant TEC. Calculations of TEC (in Step 4) have been carried out to a vertical altitude of 10000km to ensure convergence. Note also that the default altitude grid can be used in the PIM runs. The analytic fitting that is done allows for reliable (see Step 3 discussion for one caveat) extrapolation to be made to arbitrarily high altitudes.

In terms of run-time, the longest step (the most time) is the generation of the original PIM profiles.

Fitting of the PIM profiles has been performed using a variety of fit-types. As there are four profile shape parameters (three of which are independent), different possibilities exist for the amount and altitude of PIM profile information that can be fit. It was shown overall that adding "anchor" parameters did not improve fitting residuals significantly.

Step 2- Fitting in Two Dimensions

Because the spatial variations in profile parameters are smooth, polynomial fits have been sufficient to summarize the variations. In addition, IDL routines have been utilized to save time. Over a range of conditions, fourth-order fits were found to be the most reliable, as they could provide a more faithful rendition of the whole range of morphologies, without adding significantly to the runtimes.

Step 3- Regenerating Electron Densities

Here one begins at a given ground location, and along a given slant path defined by azimuth and elevation angles evaluates electron density. This is carried out as follows:

1. The first point is defined by the slant distance along the given azimuth and elevation

2. The one distance and two angles translates along a curved earth (utilizing spherical triginometry) to one distance (altitude) and two angles (offsets in latitude and longitude)

3. The six profile parameters are evaluated at the current location (given by the latitude and longitude offsets)

4. The electron density at that altitude follows directly from the six profile parameters.

One caveat has arisen. When a fit is made to an individual electron density profiles, the derived parameters always obey the rule Beta/Alpha > -Hmax. However, this is not necessarily the case when Hmax, Alpha and Beta values come from fits in two dimensions. For this reason, a watchdog is set for the parameter HFactor in the SlantPathTEC routine (see Step 4), using a previous value if the current value appears negative.

Step 4- Evaluating Slant TEC

This step includes two major issues:

- what step size should be used along the raypath ?

- what is the run-time for a single TEC calculation over a range of conditions ?

No significant downgrading of TEC estimates was seen when the step size was made coarser, from 5 to 10 to 20km, and this gives allows a little flexibility to reduce run-times should that become necessary. Actual run-times (for 408 slant TEC values) were

- fourth order fits, step size 20km, 110sec (0.25 sec/TEC)

- fourth order fits, step size 5, 450sec (1.1 sec/TEC)

- second order fits, step size 20km, 80sec (0.20 sec/TEC)

- second order fits, step size 5km, 320sec (0.80 sec/TEC).

Based on a 20km step size, the run-times are acceptably small. All software written for this project was delivered to the Air Force Research Laboratory, at Hanscom AFB.

3.2 Further Application

One project to be tackled under the auspices of the current contract is the development of a more realistic conversion between slant TEC (GPS, say) and vertical TEC. A simple conversion based on a uniform ionosphere at a (narrowly-defined) shell height is of limited validity in the equatorial region where heights vary greatly and gradients are significant.

Current work has involved the use of the profile formalism of Fox (1994) with a view to its potential applications to TEC calculations. Because the expression for electron density is both realistic (with suitably defined shape parameters, from the GTIM, say) and analytic, it can be instructive to integrate ionospheres of this numerical type and to

determine the properties of TEC from a mathematical perspective.

Commensurate with the analytic study of integrated profiles would be a study of GPS TEC morphologies, discussed briefly in section 4.1.

An additional task that this profile formalism may prove well-suited is that of real-time adjustments of the PRISM-type (see Section 2). Within the profile formalism is an iterative procedure that adjusts the internal profile scale height parameters until a match to a new (i.e. real-time) parameter is achieved. Software has already been established to use each of TEC, and a DMSP-based in situ density as the new parameter. The fact that the new GTIM includes light ions should not pose any difficulty for the formalism, because it already allows for a steady increase of scale height with altitude (as would be anticipated in the transition from O^+ to H^+).

4. IONOSPHERIC DATA ANALYSES

Significant effort in data analysis has been directed at DMSP in situ density measurements. However, this work has been described in Section 2 (model validation, 2.2, and satellite signatures, 2.4) and will not be repeated here. The following sections refer instead to studies involving foF2 and TEC databases.

4.1 Quiet-Time Variations

It was proposed in this contracted work to investigate the phenomenon of quiet-time ionospheric "dropouts", these being days when there was a significant depletion in ionospheric densities but no discernible cause (say, geomagnetic activity). Individual cases had been seen in TEC measurements made at a middle latitude station (Hamilton, MA), but no systematic study had ever been conducted.

Prior to performing a systematic search, it is essential to define what might consititute

a "dropout" event. Firstly, the geomagnetic conditions are required to be truly quiet, so that an ionospheric event could not be construed as a response to a geomagnetic disturbance. Thus, a search was first made through historical records of Kp (available on the Web at ftp://ftp.ngdc.noaa.gov/STP/GEOMAGNETIC_DATA/INDICES/KP_AP/) to locate the quietest days in each year since 1957 (the earliest foF2 data stored on the NGDC data CDROMs). The software would determine days where for N consecutive days, the maximum Kp attained was no greater than a pre-set value. Table 1 presents the results of one such search. Different search values were used in order to find the quietest days for years not represented in Table 1, and to further augment the sampling. Secondly, for all the stations with data for each of the quiet days, the diurnal maximum is compared to the median diurnal maximum for the station-month, and if it is less than 85%, the event is flagged as a "dropout". There is subsequently a visual inspection of the daily foF2 records to confirm the significance of the difference. An example is seen in Figure 17, with data from a sample of Asian stations from several days in November 1961, showing a consistent drop in diurnal maxima on day 24. Each panel in the figure shows the monthly median diurnal variation as a solid line, and the individual hourly values as plus symbols. A level of dropout is apparent in each case, and is highlighted in the figure. The histogram-like plots along the bottom of each panel denotes the 3-hourly Kp values, to define the magnetic quietness of the period.

Approximately half the CDROM foF2 database has been searched to date, and while a number of events have been catalogued, none of these has showed the same dramatic dropout seen previosuly in Hamilton-based measurements of TEC. An example of this is seen in Figure 18. The top panel shows TEC variation on May 5 and 6, 1980, plotted in sequence, while the lower panel has the two days overplotted, highlighting the dramatic nature of the dropout.

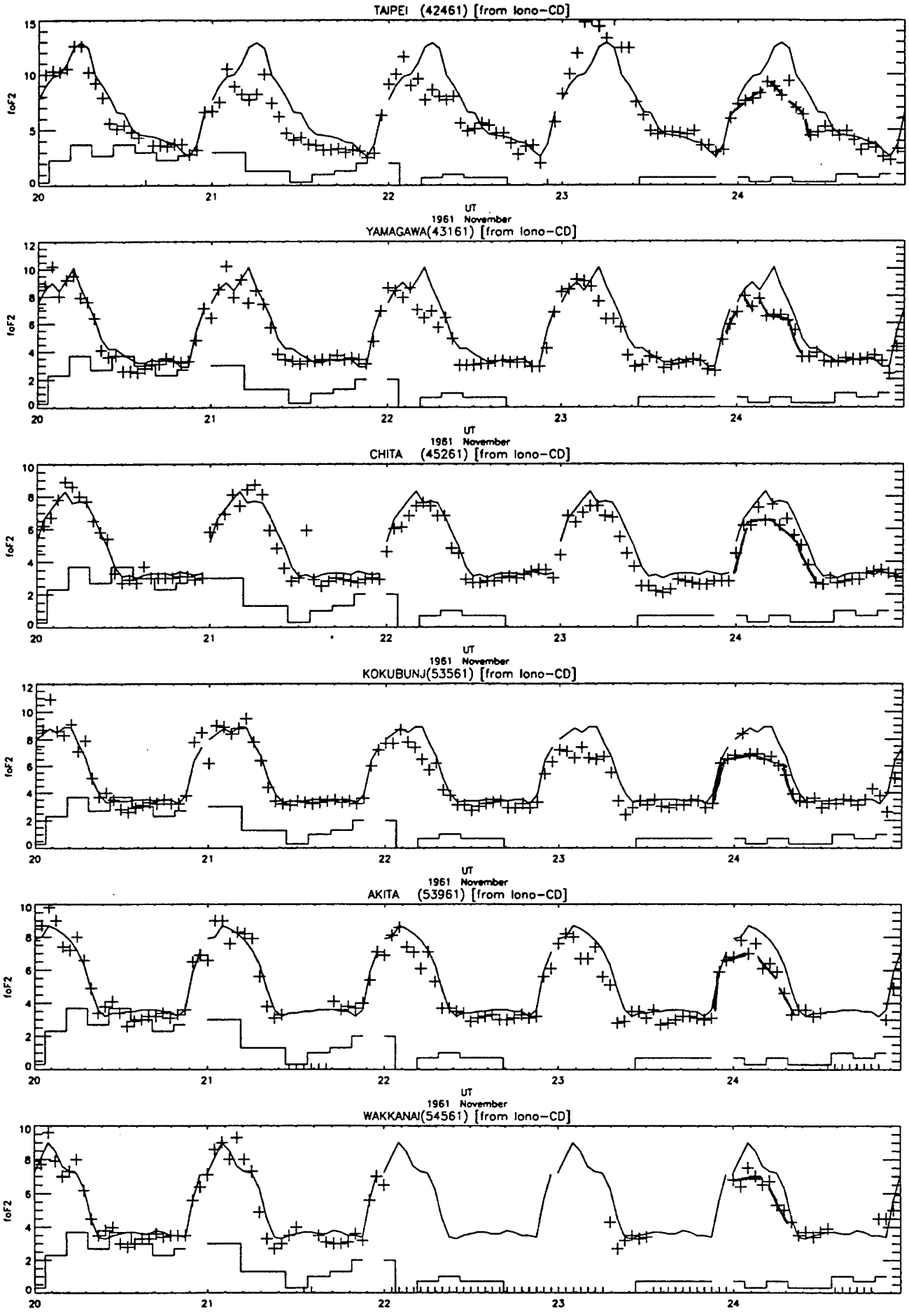
TAIPEI (42461) [from Iono-CD]
foF2
UT
1961 November
YAMAGAWA(43161) [from Iono-CD]
foF2
UT
1961 November
CHITA (45261) [from Iono-CD]
foF2
UT
1961 November
KOKUBUNJ(53561) [from Iono-CD]
foF2
UT
1961 November
AKITA (53961) [from Iono-CD]
foF2
UT
1961 November
WAKKANAI(54561) [from Iono-CD]
foF2

Figure 18.

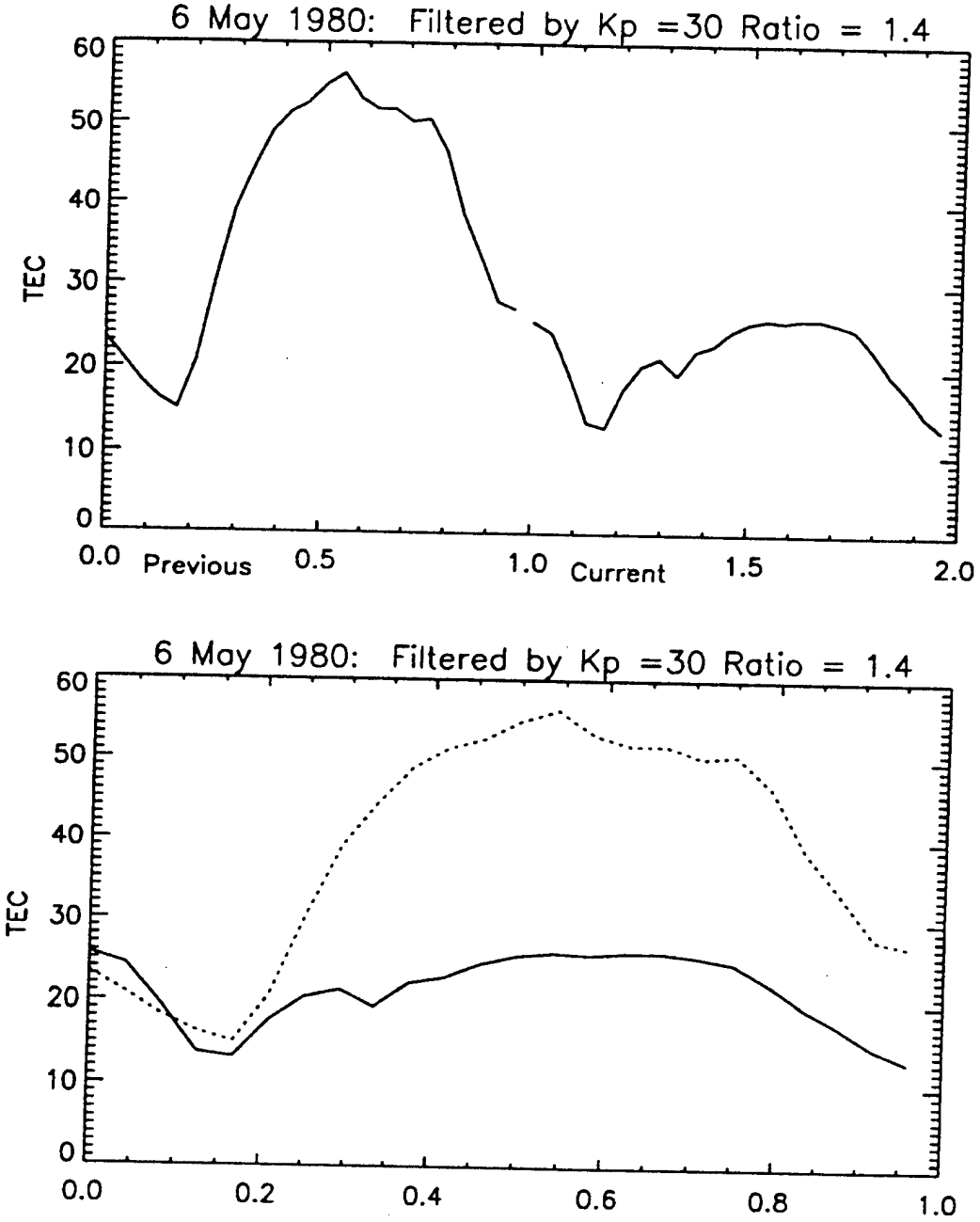
6 May 1980: Filtered by Kp =30 Ratio = 1.4
TEC
60
50
40
30
20
10
0
0.0
Previous
0.5
1.0
Current
1.5
2.0
6 May 1980: Filtered by Kp =30 Ratio = 1.4
TEC
60
50
40
30
20
10
0
0.0
0.2
0.4
0.6
0.8
1.0

This raises a question about the nature of dropouts; whether they simply reflect changes in the F region profile shape, or whether peak density changes are involved. To test this, the study will be extended to include GPS measurements. In the course of the large-scale GPS analyses discussed below, in Section 4.2, data from nearby ionosonde ground stations will be extracted and used in consort with foF2 measurements from those same epochs (say, to be downloaded from SPIDR).

Another task planned for the vast foF2 database is to define the level of quiet-time variability in the F region peak. This will again use the quietest days as defined by Kp, but will quantify the changes in foF2 at each hour of Local Time, between the current day (quiet) and the previous day (quiet). Trends will be sought in terms of season, LT, geographic region and so on. It would also be instructive to use the GTIM to determine the level of variation in the MSIS neutral winds requred for that level of variability in peak density.

4.2 Total Electron Content

The study described in Section 3.2 has a parallel in data analysis. Specifically, the question to address is how to define the range of morphologies seen in slant TEC measurments? The empirical modeling work will investigate the capabilities and ramifications of a particular type of profile shape, yet it is the real ionosphere that will ultimately define whether the model is sufficient to cover the range of variations that are observed, in order to validate its use a basis for make a slant to vertical TEC conversion.

Within the GPS database of measurements, searches will be made within various subgroups; this latter would consist variously of seasons, levels of solar activity, Local Time and locations. The goal will be to build up representative distributions of slant TEC passes against which any model can be tested. Use of coastal GPS ground stations would facilitate

testing of any slant to vertical TEC conversion, by comparisons with TOPEX TEC data, though this would be more effective at solar maximum when the relative contribution to TEC from altitudes above 1300km is smaller.

REFERENCES

Anderson, D. N., A Theoretical Study of the Ionospheric F Region Equatorial Anomaly I. Theory, *Planet. Space Sci.*, **21**, 409, 1973a

Anderson, D. N., A Theoretical Study of the Ionospheric F Region Equatorial Anomaly II. Results in the Asian and American Sectors, *Planet. Space Sci.*, **21**, 421, 1973b

Anderson, D. N., D. T. Decker and C. E. Valladares, Global Theoretical Ionospheric Model (GTIM), STEP Handbook Of Ionospheric Models Ed. R. W. Schunk, 133, 1996

Daniell, R. E., L. D. Brown, D. N. Anderson, M. W. Fox, P. H. Doherty, D. T. Decker, J. J. Sojka and R. W. Schunk, Parameterized Ionospheric Model: A Global Ionospheric Model Based on First Principles Models, *Radio Sci.*, **30**, 1499, 1995

Fejer, B. G., E. R. de Paula, R. A. Heelis and W. B. Hanson, Global Equatorial Ionospheric Vertical Plasma Drifts Measured by the AE-E Satellite, *J. Geophys. Res.*, **100**, 5769, 1995

Fejer, B. G. and L. Scherliess, Empirical Models of Storm Time Equatorial Zonal Electric Fields, *J. Geophys. Res*, **102**, 24047, 1997

Fox, M. W., A simple, convenient formalism for electron density profiles, *Radio Sci.*, **29**, 1473, 1994

Gonzalez, S. A. and M. P. Sulzer, Detection of He^+ Layering in the Topside Ionosphere Over Arecibo During Equinox Solar Minimum Conditions, *Geophys. Res. Lett.*, **23**, 2509, 1996